A postmeiotic route to stepwise polyploidy

Cintia Gómez-Muñoz[1,2], Nina Vittorelli[1,2,3], Maxime Gaudin[4], Nicolas Agier[1,2], Stéphane Delmas[1,2], Yann Corbeau[1,2], Marco Cosentino Lagomarsino[5,6], Gianni Liti[7], Bertrand Llorente[4] and Gilles Fischer[1,2]*

[1] Sorbonne Université, CNRS, Computational, Quantitative and Synthetic Biology, CQSB, F-75005 Paris, France.

[2] Sorbonne Université, CNRS, Inserm, Institut de Biologie Paris-Seine, IBPS, F-75005 Paris, France.

[3] Centre Interdisciplinaire de Recherche en Biologie, Collège de France, CNRS, INSERM, Paris, France.

[4] CRCM, Aix Marseille Université, CNRS, INSERM, Institut Paoli Calmettes, Marseille, France.

[5] IFOM-ETS, AIRC institute of molecular oncology, Milan, Italy.

[6] Dipartimento di Fisica, Università degli Studi di Milano, Milan, Italy and INFN sezione di Milano, Milan, Italy.

[7] IRCAN, CNRS, INSERM, Côte d'Azur University, Nice, France.

*Corresponding author

Email address: gilles.fischer@sorbonne-universite.fr

Abstract

Polyploidy, the presence of multiple complete chromosome sets, is a ubiquitous biological phenomenon that has played a major role in genome evolution in plants, fungi and animals. Yet the mechanisms by which autopolyploidization arises in natural populations remain incompletely understood. We identify a novel route to autopolyploidization, termed Sporulate Endoreplicate Mate (*SEM*), in which a properly reduced gamete undergoes postmeiotic endoreplication before mating with a sibling intact gamete, yielding a one-chromosome-set ploidy increase per cycle. In *Saccharomyces cerevisiae*, we experimentally demonstrate the transition from diploidy to triploidy and from triploidy to tetraploidy, positioning triploids as central intermediates in ploidy evolution rather than evolutionary dead-ends. We show that spores from intact asci can spontaneously undergo one or two successive *SEM* cycles, generating novel triploid and tetraploid strains without genetic manipulation. Natural yeast polyploids exhibit genomic signatures consistent with *SEM*, including the prevalence of triploidy, extensive aneuploidy, pervasive heterozygosity, and a strong association with heterothallism. Together, our findings establish stepwise polyploidization through iterative *SEM* cycles as the predominant natural route to polyploidy in yeast, offering a new framework for polyploid genome formation across eukaryotes.

Introduction

Polyploidy, defined as the presence of more than two complete sets of chromosomes, is widespread across the tree of life, with both ancient and recent polyploidization events documented in all major lineages (1). In plants and fungi, polyploidy promotes genomic and phenotypic diversification, facilitates adaptation to stress, and contributes to ecological success and domestication (2–5). Although less common in animals, polyploidy has played an important evolutionary role, notably through two ancient rounds of whole genome duplication (WGD) at the base of vertebrate evolution (6), and remains prevalent in fish, amphibians, and some invertebrates (7–9). Polyploidy also arises at the tissue level in multicellular organisms (1) and is a hallmark of cancer, where it fuels genome instability, tumor evolution, and therapy resistance (10–12). Overall, polyploidy is a powerful driver of genetic innovation and is increasingly recognized as a multifaceted force shaping evolution, adaptation, and disease (1, 13).

Autopolyploidization, the increase in chromosome sets within a single species, can arise through diverse mitotic or meiotic mechanisms, including somatic cell fusion, WGD through endoreplication or cytokinesis failure, polyspermy and meiotic restitution leading to unreduced gametes (1, 13, 14). Somatic genome doubling produces exclusively even ploidy states, whereas the fusion of reduced and unreduced gametes can generate triploids and other odd ploidy levels. Although triploidy has often been viewed as an evolutionary dead end due to impaired fertility, triploids can potentially serve as a bridge in the transition from diploidy to tetraploidy (13, 14).

In the budding yeast *Saccharomyces cerevisiae*, between 8% and 20% of natural isolates are autopolyploid and triploids are at least as frequent as tetraploids in natural populations (15–18), a pattern that remains difficult to reconcile with the canonical yeast life-cycle (19). Despite early reports of triploid and tetraploid isolates more than seventy years ago (20) and laboratory demonstrations that triploids can be generated through mating-based routes (21), the natural mechanism underlying triploidization in yeast remains unknown. A prevailing model posits that *S. cerevisiae* undergoes saltational transitions from diploidy to tetraploidy through

70 WGD (Fig. 1A), a view supported by the ancestral WGD event approximately 100
71 million years ago (22, 23) and observations of spontaneous autotetraploidization
72 during vegetative growth (24–26). In this framework, triploids are viewed as
73 transient intermediates arising from chromosome loss during the reversion of
74 tetraploids to diploids[31–33]. However, this model does not account for the high
75 frequency and apparent stability of triploids in natural populations (30). An
76 alternative possibility would be stepwise polyploidization through successive gains
77 of chromosome sets, in which triploids arise directly from diploids through mating
78 with haploids, rather than as derivatives of tetraploids (Fig. 1A). Although at first
79 sight such a stepwise route appears unlikely because natural diploids do not mate
80 and haploids exist only transiently between spore germination and mating, we show
81 that this double challenge is circumvented by a sequence of events that we term
82 Sporulate–Endoreplicate–Mate (*SEM*) (Fig. 1B). We demonstrate that
83 polyploidization through iterative *SEM* sequences is the predominant natural route
84 to polyploidy in *S. cerevisiae*, enabling stepwise transitions from diploidy to triploidy
85 and from triploidy to tetraploidy.

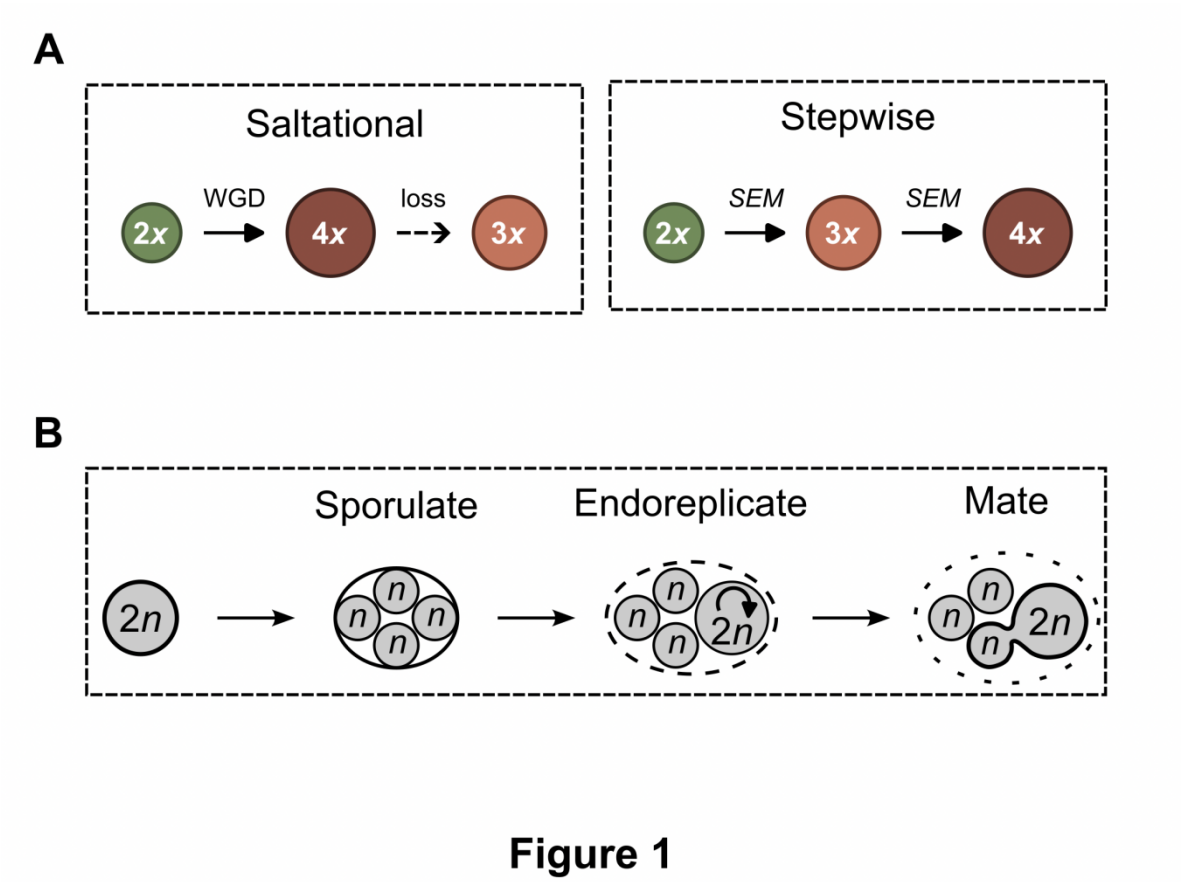

Figure 1

Figure 1: Saltational and stepwise routes to polyploidy in *S. cerevisiae*.
A, Schematic comparison between saltational and stepwise polyploidization, where *x* denotes ploidy level. In the saltational model, diploid cells (2*x*) undergo Whole Genome Duplication (WGD) to directly generate tetraploids (4*x*), whereas triploids (3*x*) arise secondarily through chromosome loss from tetraploids. In stepwise polyploidization, ploidy increases incrementally through successive Sporulate–Endoreplicate–Mate (*SEM*) cycles. **B**, Schematic representation of the *SEM* sequence, where 2*n* and *n* denote vegetative and gametic chromosome number, respectively. Sporulation of a 2*n* vegetative cell produces four 1*n* spores. Upon germination, one spore undergoes postmeiotic endoreplication, doubling the genome while preserving mating competence. Mating between the endoreplicated spore and a compatible spore from the same ascus generates a cell with increased ploidy.

Results

The Sporulate-Endoreplicate-Mate sequence. In this study, we follow the terminology of Ramsey & Schemske (14), where $2n$ refers to the vegetative chromosome number and n to the gametic chromosome number, independently of ploidy. Ploidy levels are indicated by x, with diploids, triploids, and tetraploids corresponding to $2x$, $3x$, and $4x$, respectively.

The *SEM* sequence describes a succession of events that begins with *S,* the sporulation of a $2n$ vegetative cell which produces four $1n$ spores enclosed within an ascus (Fig 1B). This is followed by *E*, an endoreplication event that occurs postmeiotically upon spore germination. Here, endoreplication is used as a generic term encompassing both endocycling and endomitosis (31, 32), reflecting the fact that the exact molecular mechanism underlying genome doubling is currently unknown. Endoreplication of a germinating spore generates a cell with a duplicated genome and carrying a single mating type that is thus capable of mating, while the ascus environment concomitantly supplies a compatible non-duplicatd partner. The final event is *M,* the mating between the endoreplicated spore and a compatible spore from the same ascus, resulting in a cell carrying a $+1x$ ploidy increment (Fig. 1B). Each iteration of the *SEM* sequence increases ploidy by one chromosome set (Fig. 1A).

Below, we provide experimental evidence for each step of *SEM* sequence. Additionally, we were able to experimentally recapitulate the full process of stepwise ploidy increases $2x \rightarrow 3x \rightarrow 4x$ through two iterations of the *SEM* sequence. Importantly, the stepwise polyploidization model predicts the frequent emergence of both triploids and tetraploids and suggests that increasing ploidy above $4x$ is rare. Finally, we verified that the genomic characteristics of most natural polyploids are fully compatible with their stepwise origin and that the saltational route accounts for a minority of cases.

Stepwise diploid-to-triploid transition. Iteration one of the *SEM* sequence starts with *S1* the sporulation of a diploid parental cell and is directly followed by *E1* the endoreplication of one of the germinating spores (Fig. 2A). Previous studies showed

130 that endoreplication occurs frequently in vegetative cells, with approximately 17%
131 of haploids spontaneously diploidizing after 100 generations in the absence of
132 external stress, and can even reach 100% in the presence of EtOH or KCl (33).
133 Endoreplicated strains are fully homozygous across the entire genome, hence carry
134 a single mating type enabling them to mate.
135 To detect endoreplication in natural populations, we screened a collection of 742
136 natural diploids using a combination of mating assays (Extended Methods) to
137 identify endoreplicated strains capable of mating but persisted without finishing the
138 *SEM* sequence. As expected, most strains exhibited no or extremely low levels of
139 mating activity. Nevertheless, a subset of strains showed clear and reproducible
140 mating signals (Table S1, Fig. 2B). We further characterized these strains by PCR
141 genotyping the *MAT* locus. We identified 26 single mating type diploids capable of
142 mating. About half of these were heterozygous at the genome level, suggesting they
143 arose through *MAT* locus hemizygotization or homozygotization (Fig. 2B). These
144 strains could contribute to polyploidization upon outcrossing, independently from
145 the *SEM* sequence. The other eleven strains were fully homozygous, indicating that
146 they most likely resulted from endoreplication (Fig. 2B). They belong to eight
147 different clades suggesting that endoreplication is pervasive across *S. cerevisiae*
148 populations (Table S1).
149 This initial screen provides clear evidence that spontaneous endoreplication occurs
150 at measurable frequencies in natural yeast populations. To determine whether
151 postmeiotic endoreplication can occur concomitantly with spore germination, as
152 proposed for the *E1* step of the *SEM* sequence (Fig. 2A), we screened 23 homothallic
153 and 9 heterothallic diploid strains for their capacity to undergo spontaneous spore
154 endoreplication. We sporulated all 32 strains, measured the ploidy by flow
155 cytometry of 684 microdissected spores from their meiotic progeny, and determined
156 their mating genotype (Table S2, Table S3). Homothallic diploids produce haploid
157 spores that self-mate through mating-type switching, generating *MATa*/*MATα*
158 diploid monosporic isolates. As expected, all 23 homothallic diploids produced
159 exclusively *MATa*/*MATα* diploid monosporic isolates, and none showed evidence
160 of endoreplication, which would have resulted in tetraploid monosporic isolates

161 (Fig. 2C). In contrast, heterothallic diploids produce haploid spores that cannot
162 switch mating-type and therefore develop into single-mating-type haploid
163 monosporic isolates. Consistent with this expectation, all heterothallic strains
164 produced single–mating-type haploid monosporic isolates (Fig. 2C). Notably, five
165 of the nine heterothallic strains also produced ~2*x* single-mating-type monosporic
166 isolates, suggesting that endoreplication occurred after spore germination.
167 We next tested whether these putatively endoreplicated isolates were able to
168 generate triploid strains by crossing them with compatible haploid testers
169 (corresponding to the *M1* step in Fig. 2A). The ~2*x* monosporic isolates derived from
170 the two heterothallic strains AKR and ALH, both belonging to the Asian
171 fermentation clade, produced triploid progeny upon mating, confirming that these
172 isolates were endoreplicated (Supplementary Fig. 1).
173 Together, these results demonstrate that (i) a subset of natural diploid isolates likely
174 originates from haploid endoreplication, (ii) endoreplication can occur upon spore
175 germination, and (iii) endoreplicated isolates are capable of generating triploid
176 strains. These findings further reinforce the strong association between
177 heterothallism and natural polyploidy (34), as only heterothallic diploids generated
178 triploid isolates through the *SEM* pathway.

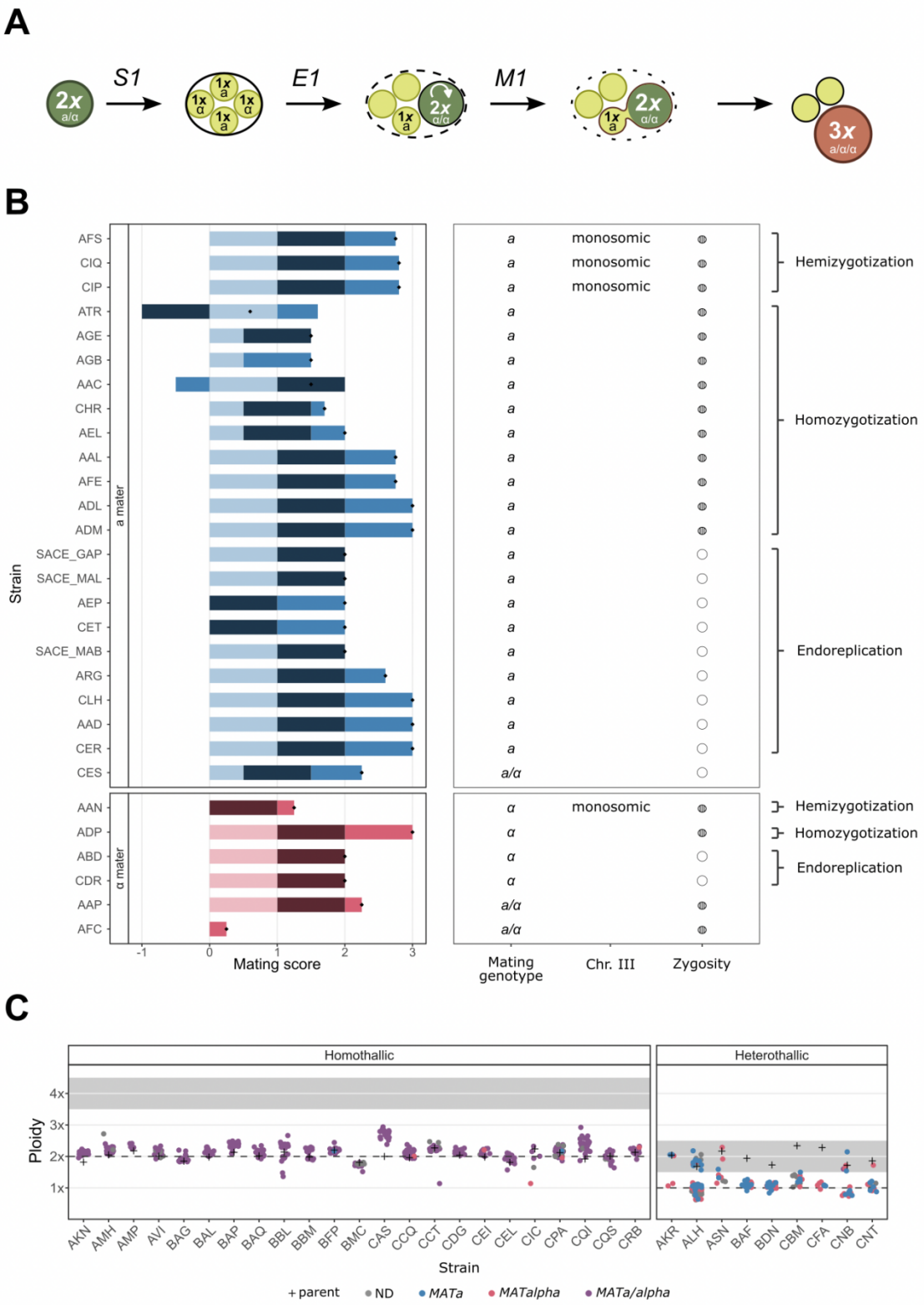
A
S1
E1
M1
2x a/α
1x a
1x α
2x α/α
3x a/α/α
B
Strain
a mater
α mater
AFS
CIQ
CIP
ATR
AGE
AGB
AAC
CHR
AEL
AAL
AFE
ADL
ADM
SACE_GAP
SACE_MAL
AEP
CET
SACE_MAB
ARG
CLH
AAD
CER
CES
AAN
ADP
ABD
CDR
AAP
AFC
-1
0
1
2
3
Mating score
a
monosomic
a/α
α
Mating genotype
Chr. III
Zygosity
Hemizygotization
Homozygotization
Endoreplication
C
Homothallic
Heterothallic
Ploidy
4x
3x
2x
1x
AKN
AMH
AMP
AVI
BAG
BAL
BAP
BAQ
BBL
BBM
BFP
BMC
CAS
CCQ
CCT
CDG
CEI
CEL
CIC
CPA
CQI
CQS
CRB
AKR
ALH
ASN
BAF
BDN
CBM
CFA
CNB
CNT
Strain
+ parent
ND
MATa
MATalpha
MATa/alpha

Figure 2

Figure 2: Endoreplication during spore germination enables diploid-to-triploid transition
A, Schematic of the first iteration of the *SEM* sequence, in which sporulation (*S1*), endoreplication (*E1*), and mating (*M1*) collectively enable the transition from diploid to triploid. **B**, Identification of natural diploid strains capable of mating. Mating scores include mass mating assays (medium shading), observation of zygote formation (dark shading) and creeping phenotypes (light shading), revealing a subset of diploid isolates exhibiting reproducible mating activity, as *a*-mater (blue) or *α*-mater (red). *MAT* locus hemizygotization corresponds to chromosome III monosomy. Genome-wide homo and heterozygosity are symbolized by open and stripped circles, respectively. Fully homozygous single-mating-type diploids are inferred to result from haploid endoreplication. **C**, Ploidy and mating-type composition of monosporic isolates derived from homothallic and heterothallic diploid strains. Homothallic strains produce exclusively *MATa*/*MATα* diploids (purple), whereas heterothallic strains generate haploid *MATa* (blue) or *MATα* (pink). Black crosses indicate parental strain ploidy. The shaded area indicates the ploidy range expected from endoreplication. Several heterothallic diploids produce monosporic isolates consistent with endoreplication. The homothallic CAS strain produces monosporic isolates showing increased ploidy compared to the parental, although lower than expected for endoreplication.

Stepwise triploid-to-tetraploid transition. The second iteration of the *SEM* sequence allows stepwise acquisition of tetraploidy and begins with *S2*, the sporulation of a triploid parental cell (Fig. 3A). Among 46 triploids from the 1,011 collection, 38 (87.5%) were able to sporulate, with efficiency ranging from 3% to 97% (median 44%) (35). We microdissected 180 spores from the meiotic progeny of each of three representative euploid triploid strains and confirmed that spore viability was extremely low (5.0–7.8%; Supplementary Fig. 2, Table S3). This could be due to chromosome missegregation or mutational load. To disentangle their respective contribution, we constructed a fully homozygous triploid strain (AKN-3*x*) and measured its gamete viability. This artificial triploid showed 56.7% gamete viability (Supplementary Fig. 2), versus 96% in the original AKN diploid strain (Table S3), indicating that segregation defects alone reduce fertility by approximately 2-fold in triploids, as previously reported (36). The even lower viability of natural triploids (5.0–7.8%) highlights the additional contribution of mutational load in their genomes, estimated to comprise several heterozygous high-impact variants in essential genes (37).

Because triploid cells carry an odd number of homologs for each chromosome, segregation at meiosis I is necessarily unbalanced, and triploid meiosis is therefore expected to produce spores with variable chromosomal contents ranging from 1*x* to 3*x* (expected mean 1.5*x*, Fig. 3A). Genome sequencing of 32 monosporic isolates from

216 three natural euploid triploids showed that all spore genomes were aneuploid, *i.e.*
217 none were perfectly haploid, diploid or triploid (Fig. 3B; Table S2).
218 We identified genomic signatures of *E2*, the postmeiotic endoreplication step of the
219 second iteration of the *SEM* sequence (Fig. 3A), in six of the 32 sequenced
220 monosporic isolates (Supplementary Fig. 3). First, these isolates contain multiple
221 chromosomes present in four copies (Fig. 3B). Because regular meiotic segregation
222 of parental triploid genomes can generate at most three copies of a chromosome per
223 spore, tetrasomes are most parsimoniously explained by endoreplication of
224 originally disomic chromosomes. Second, these six isolates are completely devoid of
225 monosomes, in contrast to their widespread presence in non-endoreplicated spores,
226 suggesting that all originally monosomic chromosomes were converted into
227 disomes by endoreplication (Fig. 3B). Third, allele balance ratios (*ABRs*) at
228 heterozygous sites show ~50% heterozygosity for tetrasomes and complete
229 homozygosity for disomes in all six isolates, as expected under endoreplication,
230 although three isolates also exhibit additional *ABR* complexity affecting a small
231 number of chromosomes (Fig. 3C, Supplementary Fig. 3). Additionally, the six
232 isolates exhibited ploidy levels ranging from 2.2*x* to 3.0*x* (mean 2.6*x*), significantly
233 higher than the 1.1*x* to 2.4*x* range (mean 1.7*x*) observed in the other isolates (Fig. 3D).
234 Together, these findings indicate that postmeiotic endoreplication occurs at
235 appreciable frequency in triploid progeny (6 of 32, 19%), supporting the
236 endoreplicate step of the second iteration of the *SEM* sequence (Fig. 3A).
237 We assessed the mating ability of the six endoreplicated monosporic isolates, along
238 with 26 non-endoreplicated isolates, by genotyping their mating types and
239 evaluating mating proficiency using mass mating assays. Five of the six isolates
240 behaved as *MATα* strains, while the remaining one was a non-mater (Table S2). To
241 validate the *M2* step of the *SEM* sequence (Fig. 3A), we crossed the five mating-
242 competent endoreplicated isolates with a haploid tester strain and measured the
243 ploidy of the resulting progeny. All crosses resulted in increased ploidy, with
244 increments ranging from +0.7*x* to +2.1*x*, demonstrating the stepwise transition from
245 triploidy to tetraploidy (Supplementary Fig. 4).

Together, these results show that triploid sporulation is frequent but inefficient, producing few viable spores. Nonetheless, these viable progenies are highly aneuploid, often undergo postmeiotic endoreplication, and can act as mating-competent partners, enabling stepwise increases in ploidy toward tetraploidy.

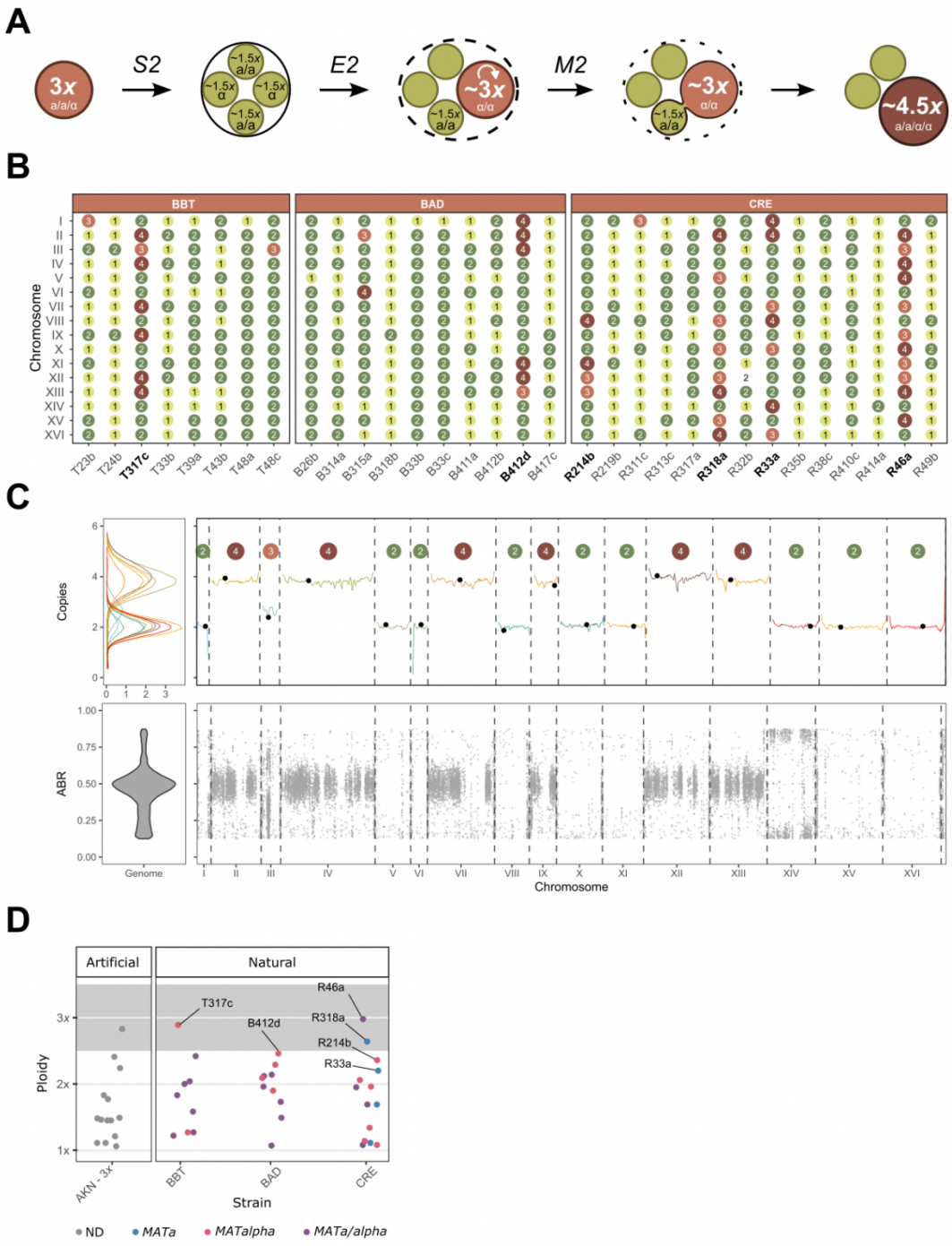
A
3x
a/a/α
S2
~1.5x
a/a
~1.5x
α
E2
~3x
α/α
M2
~4.5x
a/a/α/α
B
BBT
BAD
CRE
Chromosome
C
Copies
ABR
Genome
Chromosome
D
Artificial
Natural
Ploidy
Strain
AKN - 3x
BBT
BAD
CRE
T317c
B412d
R46a
R318a
R214b
R33a
ND
MATa
MATalpha
MATa/alpha

Figure 3

250

251 **Figure 3: Stepwise triploid-to-tetraploid transition through the second iteration of the SEM**
252 **sequence.**
253 **A**, Schematic of the second *SEM* iteration (*S2–E2–M2*) initiated by sporulation of a triploid parental
254 strain. Triploid meiosis produces highly aneuploid spores with variable chromosome copy numbers
255 that average to 1.5*x*. The mating genotype of the parental triploid strain is *MATa*/*α*/*α*. **B**, Chromosome
256 copy number profiles of 32 monosporic isolates derived from triploid meiosis, showing extensive
257 aneuploidy. Six isolates (bolded names) display tetrasomic chromosomes as well as complete absence
258 of monosomic chromosomes, indicative of postmeiotic endoreplication. **C**, Genome-wide (left) and
259 chromosome-level (right) copy number (top) and allele balance ratio (*ABR*; bottom) profiles of the
260 T317c monosporic isolate. Chromosome copy numbers correspond to the sequencing depth
261 normalized by the genome ploidy. Centromeres are marked with black circles and the rounded
262 chromosome copy number is indicated in colored circles. In *ABR* profiles, only alternative alleles are
263 plotted. **D**, Inferred ploidy distributions of monosporic isolates, highlighting increased ploidy in
264 endoreplicated progeny (the 6 isolates in bold in panel B are highlighted). The shaded area indicates
265 the approximate ploidy range expected from endoreplication in monosporic isolates.

266 **Spontaneous generation of novel polyploids through stepwise polyploidization.**
267 A key assumption of the *SEM* model is that postmeiotic endoreplication and mating
268 occur sequentially and rapidly after spore germination within the same ascus. To
269 directly test this prediction, we designed an experimental system in which diploid
270 strains were sporulated and intact asci, *i.e.* without spore dissection, were
271 individually micromanipulated and plated onto rich medium. This setup allowed
272 spore germination, potential endoreplication, and intra-ascus mating to occur
273 spontaneously under laboratory conditions, after which ascus viability was assessed
274 and the ploidy of the resulting colonies was determined (Fig. 4A, Table S4).
275 We micromanipulated asci from 12 diploid strains naturally defective for mating
276 type switching due to loss of function mutations in the *HO* gene. We focused on
277 heterothallic strains because most natural polyploids also lack a functional *HO* gene
278 (34), and because our results showed that only heterothallic spores endoreplicated
279 (Fig. 2C). These strains span a broad genetic diversity, having been isolated from
280 both natural and anthropologic niches across multiple geographic regions (Table
281 S2). In total, we micromanipulated 1,191 intact asci (50 - 150 asci per strain). Ascus
282 viability varied widely among strains (Fig. 4B). We recovered both haploid and
283 diploid monoascus isolates. Haploid monoascus isolates corresponded to unmated
284 monosporic progeny, whereas diploid isolates most likely resulted from intra-ascus
285 mating between compatible spores (Fig. 4B). Notably, five of the twelve tested
286 diploid strains produced triploid monoascus isolates at frequencies ranging from

287 1.2% to 9.1% (Fig. 4B). In total, nine triploid isolates were recovered, subcloned, and
288 confirmed as triploid by both flow cytometry and whole-genome sequencing (Table
289 S4 and S5). Chromosome copy number and *ABR* profiles displayed values
290 characteristic of triploidy (Supplementary Fig. 6). Together, these results
291 demonstrate that sporulation of a heterothallic diploid strain can spontaneously
292 generate novel triploid progeny through at least one complete iteration of the *SEM*
293 sequence (Fig. 2A).
294 We next tested whether these newly formed triploids could undergo a second
295 iteration of the *SEM* sequence and spontaneously generate tetraploid progeny. A
296 randomly selected novel triploid isolate from each of two genetic backgrounds
297 (ALH and CNT) was resporulated. In both cases, ascus viability was reduced
298 relative to the diploid parent, consistent with impaired triploid meiosis (Fig. 4C).
299 The resulting monoascus isolates displayed a range of ploidies, including haploid
300 and diploid isolates, indicating that ploidy often regressed through meiosis as
301 expected. However, other isolates were triploid, suggesting that ploidy was restored
302 through sporulation followed by mating within the same ascus (Fig. 4C).
303 Importantly, the triploid isolates generated in this process carry novel allelic
304 combinations relative to their parental genotypes and potentially altered aneuploidy
305 landscapes resulting from meiotic resegregation of trivalents. Thus, even without
306 further increase in ploidy, these isolates enable exploration of novel genotypic space.
307 Notably, among the ascus progeny of ALH-3*x*, we identified a tetraploid isolate
308 (ALH-4*x*; Fig. 4C). This isolate was subcloned, and its ploidy was validated by both
309 flow cytometry and whole-genome sequencing (Fig. 4D and E). Comparison of
310 chromosome *ABR* profiles between ALH-3*x* and ALH-4*x* revealed the expected +1*x*
311 increase in genome content, providing direct evidence that ploidy can further
312 increase through a second iteration of the SEM sequence (Fig. 3A).
313 Together, these results demonstrate that the entire ploidy transition, from diploid to
314 tetraploid through intermediate triploid states, can be fully recapitulated under
315 laboratory conditions and harnessed to generate polyploids with novel genetic
316 compositions.

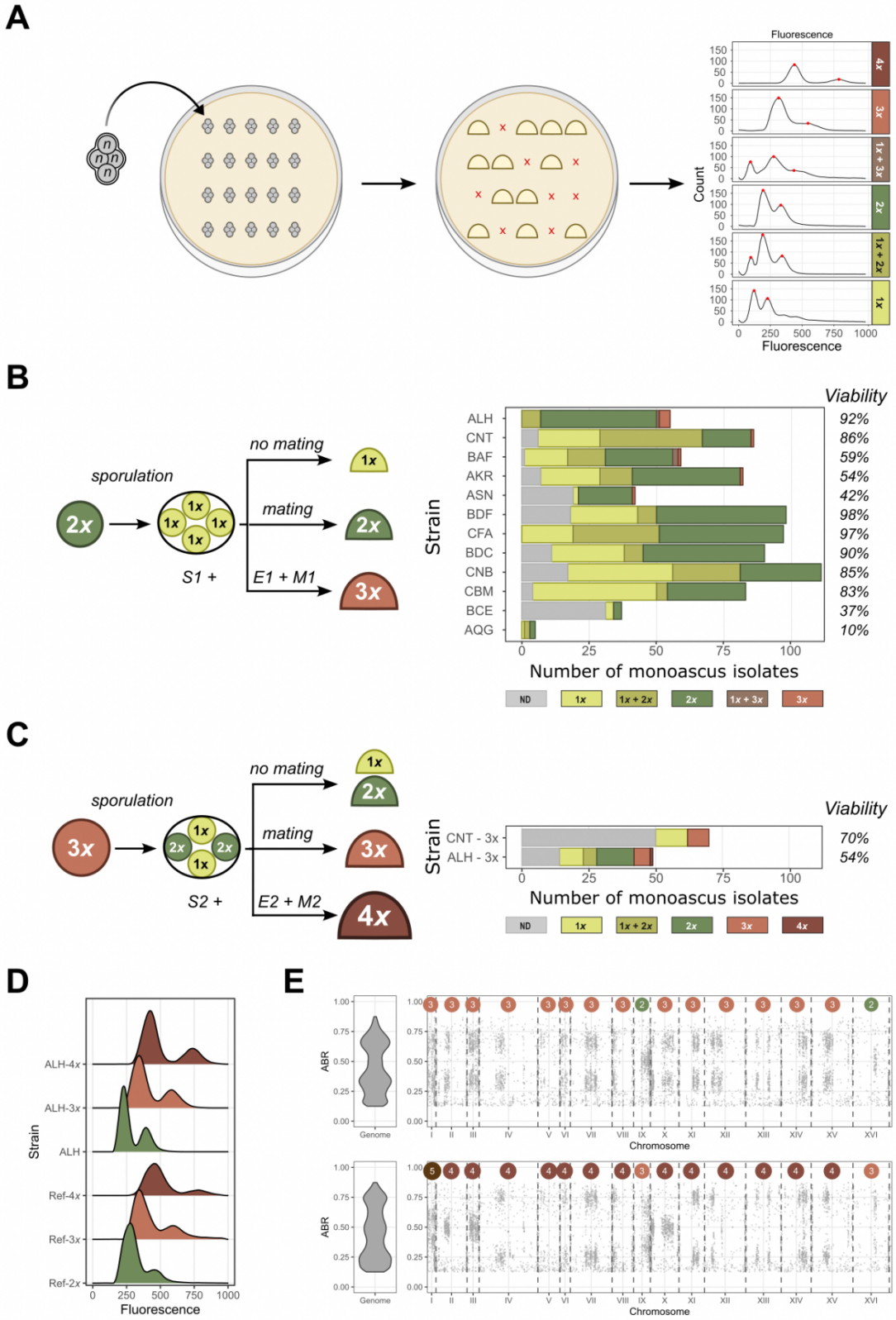
A
Fluorescence
Count
4x
3x
1x + 3x
2x
1x + 2x
1x
Fluorescence
B
sporulation
2x
1x
S1 +
no mating
mating
E1 + M1
Viability
Strain
ALH 92%
CNT 86%
BAF 59%
AKR 54%
ASN 42%
BDF 98%
CFA 97%
BDC 90%
CNB 85%
CBM 83%
BCE 37%
AQG 10%
Number of monoascus isolates
ND
1x
1x + 2x
2x
1x + 3x
3x
C
sporulation
3x
2x
S2 +
no mating
mating
E2 + M2
4x
Viability
CNT - 3x 70%
ALH - 3x 54%
Number of monoascus isolates
D
Strain
ALH-4x
ALH-3x
ALH
Ref-4x
Ref-3x
Ref-2x
Fluorescence
E
ABR
Genome
Chromosome

Figure 4

318 **Figure 4 | Spontaneous generation of novel polyploids through iterative *SEM* cycles.**
319 **A**, Experimental design for intact ascus micromanipulation, allowing spore germination,
320 endoreplication, and intra-ascus mating to occur without spore dissection. Viable asci form colonies
321 whose ploidy is determined by flow cytometry. Histograms on the right correspond to DNA content
322 measurements from representative colonies, and are not schematic. **B**, Ploidy outcomes of monoascus
323 isolates derived from heterothallic diploid strains. Triploid isolates (3*x*) arise spontaneously in
324 multiple genetic backgrounds, consistent with completion of the first *SEM* iteration. In some cases,
325 monoascus isolates exhibited mixed ploidies within the colony, with haploid and diploid, or haploid
326 and triploid cells coexisting within the same colony (1*x*+2*x* or 1*x*+3*x*). In other instances, ploidy could
327 not be reliably determined (ND) due to slow growth or multicellular clumping, a phenotype
328 frequently observed in wild strains (38). **C**, Resporulation of newly formed triploids generates a
329 spectrum of ploidy outcomes (identical to B), including tetraploidy (4*x*), demonstrating completion
330 of the second *SEM* iteration. **D**, DNA content of ALH, ALH-2*x* and ALH-3*x* measured by cytometry.
331 The reference strains used to calibrate ploidy are the laboratory strain BY4743 (2*x*), the natural triploid
332 CRE (3*x*) and the artificial tetraploid AKN-4*x*. **E**, Genome-wide (left) and chromosome-level (right)
333 allele balance ratio (*ABR)* profiles for ALH-3*x* (top) and ALH-4*x* (bottom). Chromosome copy
334 numbers corresponding to the sequencing depth normalized by the genome ploidy are indicated in
335 colored circles.

336 **A barrier to increase ploidy beyond tetraploidy.** We explored whether further
337 stepwise ploidy increase beyond tetraploidy was achievable through the *SEM*
338 sequence. We found that 25 of 38 (65.8%) tetraploids efficiently sporulate as 25 of 38
339 (65.8%) were able to sporulate, with a median efficiency of 57% (35). Using two
340 representative strains, we confirmed the low spore viability of tetraploids (6.7% to
341 12.2%, Supplementary Fig. 2). We constructed an artificial homozygous tetraploid
342 (AKN-4*x*) to estimate gamete viability in the absence of deleterious recessive
343 mutations. This strain showed 77.2% spore viability, significantly higher than the
344 56.7% in the homozygous triploid AKN-3*x* (Supplementary Fig. 2), showing that
345 chromosome segregation is less affected in tetraploid than in triploids, as previously
346 reported (39). Consistently, genome sequencing of 28 monosporic isolates obtained
347 in the meiotic progeny of two natural euploid tetraploids revealed very few
348 monosmic chromosomes as well as a much lower global incidence of aneuploidies
349 than in triploid progenies (Supplementary Fig. 5A). Eleven isolates were euploid
350 diploids while the remaining showed either monosomies (in seven cases) and/or
351 trisomies (in 14 cases). Thus, the low spore viability of tetraploids probably reflects
352 the major contribution of recessive mutational load exposed at homo- or
353 hemizygous state in the gametes. No sign of spore endoreplication was detected in
354 the progeny of tetraploids, suggesting that further ploidy increase through the *SEM*

355 sequence is limited, or at least less frequent than in the progeny of triploids
356 (Supplementary Fig. 5B). Monosporic isolates displayed various mating-type
357 combinations associated with complex mating phenotypes (Supplementary Fig. 5B
358 and 5C, Table S3), including bisexual mating (40) and dioecy (41).
359 Finally, genome sequencing of 16 monosporic isolates obtained in the meiotic
360 progeny of one natural pentaploid revealed consistent segregation of disomes and
361 trisomes across all isolates (a single case of monosomic chromosome I was observed,
362 Supplementary Fig. 5A). No sign of spore endoreplication was detected in the
363 progeny of the pentaploid strain.
364 In conclusion, we found no evidence supporting stepwise ploidy increase beyond
365 tetraploidy, suggesting that 4*x* might represent an upper limit for this process. This
366 is consistent with the rarity of natural pentaploids, which encompass only about
367 0.2% of strains in the largest available collection (18), and with the absence of
368 hexaploid or higher-ploidy isolates.
369
370 **Stepwise polyploidization as the main route to natural polyploidy.** The stepwise
371 and saltational routes to polyploidization rely on distinct mechanisms, namely the
372 *SEM* sequence and the WGD, respectively (Fig. 1), and are therefore expected to
373 leave contrasting genomic signatures. To discriminate between these modes of
374 origin, we analyzed the genomic constitution of the 91 natural polyploids from the
375 1,011 collection (16) and assessed whether their features are more consistent with a
376 stepwise or a saltational process.
377 We first measured the DNA content of the 91 natural polyploids by flow cytometry
378 and inferred ploidy without rounding to integer values. Rather than forming
379 discrete clusters corresponding to strict 3*x*, 4*x*, or 5*x* ploidy levels, the data revealed
380 an almost continuous ploidy range from 2.5*x* to 5.5*x* (Fig. 5A, Table S6), with clear
381 discontinuities near 3.5*x* and 4.5*x* delimiting triploid, tetraploid, and pentaploid
382 classes. Independent analysis of genome-wide *ABRs* at heterozygous sites yielded
383 ploidy estimates largely concordant with DNA content, with only three exceptions
384 (ASA, BEM, and CBR; Fig. 5A). This integrated reassessment led us to reclassify two
385 previously reported tetraploids (AFT and CFS) as triploids and to resolve one

386 previously ambiguous strain (AEC) as a tetraploid, resulting in a final dataset
387 comprising 48 triploids, 38 tetraploids, and 5 pentaploids (Table S6).
388 Under a saltational polyploidization model, the prevalence of triploids would
389 require chromosome loss from tetraploids to occur more frequently than WGD from
390 diploids. Although rapid chromosome loss has been documented in laboratory
391 engineered homozygous tetraploids (27–29), it typically results in diploid rather
392 than triploid genomes (2). Moreover, long term vegetative propagation of natural
393 tetraploids revealed no reduction in ploidy, indicating that polyploid levels are
394 stable in natural isolates (30). Together, these observations argue against a dominant
395 saltational origin and instead support a stepwise route to polyploidization. This
396 conclusion is further reinforced by the strong enrichment of heterothallic strains
397 among natural polyploids (34), which is expected under the *SEM* model given that
398 endoreplication is restricted to heterothallic spores (Fig. 2C).
399 Additional genomic features are likewise inconsistent with a WGD-based origin. If
400 WGD is independent from zyogosity, a saltational model predicts that the fraction
401 of homozygous polyploids should be comparable to that observed among diploids
402 (47% in the 1,011 collection (16)). In contrast, we detected only two homozygous
403 triploids and no homozygous tetraploids among the 91 natural polyploids.
404 Furthermore, WGD of a heterozygous diploid genome would produce tetraploids
405 characterized by a dominant *ABR* peak near 0.5 (Supplementary Fig. 7), a signature
406 that is never observed in our data (Fig. 5B), providing strong evidence against WGD
407 as the primary mechanism of tetraploidization.
408 Finally, combining chromosome-specific sequencing coverage with *ABRs* revealed
409 extensive aneuploidy among natural polyploids, including 122 whole-chromosome
410 and 63 segmental aneuploidies (Table S6, Fig. 5C). Under the *SEM* model, such
411 aneuploidy is expected to accumulate with increasing ploidy, as tetraploids and
412 pentaploids originate from highly aneuploid spores produced by triploid meiosis.
413 In contrast, a saltational route predicts higher aneuploidy levels in triploids arising
414 from chromosome loss in tetraploids. Consistent with the stepwise model, we
415 observed a monotonic increase in the proportion of aneuploid strains with ploidy,
416 from 52% in triploids to 78% in tetraploids and 100% in pentaploids.

417 Together, these complementary genomic signatures indicate that higher ploidy
418 levels in *S. cerevisiae* arise predominantly through iterative cycles of the *SEM*
419 sequence rather than through saltational whole-genome duplication, establishing
420 stepwise polyploidization as the main evolutionary route to natural polyploidy.

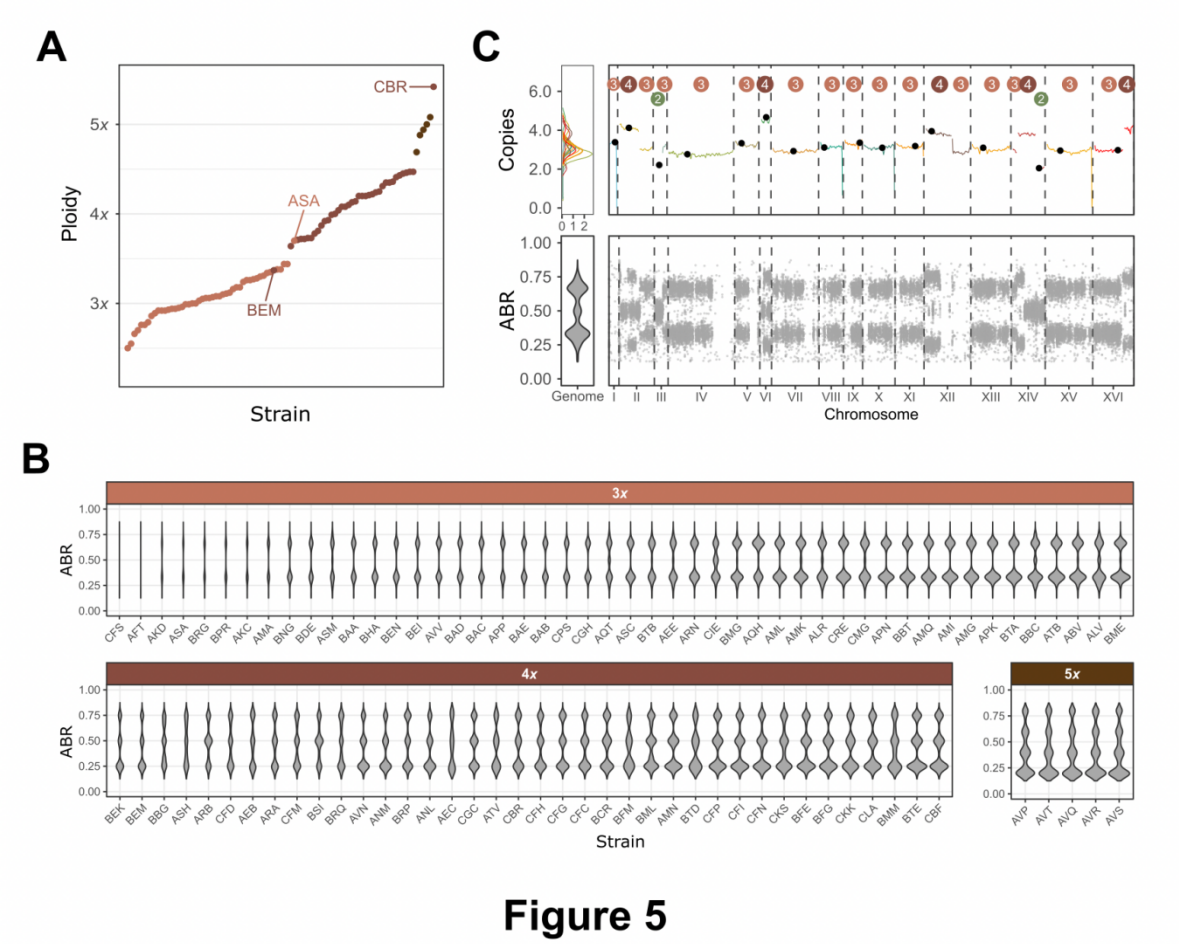

Figure 5

421

422 **Figure 5 | Genomic signatures of natural polyploids support a stepwise origin.**
423 **A**, Ploidy estimates of 91 natural polyploid isolates inferred from flow cytometry, showing a near-
424 continuous distribution from ~2.5*x* to ~5.5*x* with discontinuities delineating triploid, tetraploid, and
425 pentaploid classes. **B**, Genome-wide allele balance ratio (*ABR*) distributions for the 91 natural
426 polyploids. Observed *ABR* patterns are inconsistent with whole-genome duplication of heterozygous
427 diploids and instead support stepwise ploidy increase. **C**, Chromosome copy number and *ABR*
428 profiles of a representative natural polyploid strain (AQT) presenting several whole-chromosome
429 and segmental aneuploidies.

Discussion

Here, we identify a natural route to polyploidization in yeast that we term stepwise polyploidization, mediated by iterative cycles of the *SEM* sequence. This route begins with sporulation, followed by postmeiotic endoreplication during spore germination. The sequence ends with mating between the endoreplicated spore and a compatible meiotic product within the ascus. This process contrasts sharply with the somatic WGD in diploids, which is often invoked to explain polyploid formation in yeast, as well as with the dominant mechanism described in plants, which relies on the fusion of unreduced gametes produced by meiotic restitution (14). Notably, a conceptually related process has been proposed in plants, where a subset of $2x$ nuclei in mature pollen may arise from mitotic endoreplication after completion of meiosis rather than from meiotic restitution (42). This conceptual parallel suggests that postmeiotic endoreplication may contribute to polyploid formation beyond fungi.

The *SEM* model provides a unified explanation for several genomic characteristics of natural yeast polyploids, including strong association with heterothallism, pervasive heterozygosity, frequent triploid state and extensive aneuploidy. In a recent work, we showed that natural polyploidy in yeast was strongly associated with repeated losses of self-fertility (34), yet the causal basis of this association remained unclear. Our results provide a mechanistic explanation: only heterothallic spores experience a prolonged single–mating-type state upon germination that permits endoreplication, whereas homothallic spores rapidly self-mate and therefore do not enter the *SEM* pathway. At the same time, ploidy increases through mating between genetically distinct meiotic products preserve heterozygosity and account for the observed allele-balance distributions, in contrast to duplication of a single diploid genome. Stepwise polyploidization further implies that triploids are not rare anomalies but expected and stable intermediates produced by a single iteration of the *SEM* sequence. Because meiosis in triploids is intrinsically unbalanced, viable progeny are highly aneuploid, providing a direct explanation for the extensive aneuploidy observed in tetraploids. Given the broad ploidy range of

460 spores produced by triploid meiosis, pentaploids could theoretically be generated
461 by mating between an endoreplicated ~3*x* spore and a near-diploid partner.
462 The postmeiotic endoreplication step itself emerges as the pivotal mechanism of
463 stepwise polyploidization. Although the precise molecular mechanisms underlying
464 spontaneous spore endoreplication remain to be elucidated, an early study
465 identified a mutation in *CDC31*, a gene required for spindle pole body duplication,
466 as a driver of endoreduplication (43). To date, at least 16 genes have been implicated
467 in ploidy increase in *S. cerevisiae* (44). These genes encode proteins that primarily
468 regulate spindle pole body duplication, chromosome segregation, cytokinesis and
469 cell-cycle control, thereby highlighting the central role of cell-division and genome-
470 partitioning pathways in the control of ploidy. Moreover, high rate of
471 endoreplication depends on the presence of a functional copy of *SSD1*, a gene that
472 also regulates aneuploidy tolerance in wild yeast (45, 46). Future work will be
473 required to assess the extent of natural variation in these genes across populations
474 and to dissect the molecular events governing genome doubling associated with
475 spore germination.
476 In conclusion, our findings demonstrate that stepwise polyploidization through
477 iterative cycles of the *SEM* sequence constitutes the predominant route to natural
478 polyploidy in *S. cerevisiae*, although alternative routes, such as those involving
479 mating-competent diploids arising from *MAT* hemi- or homozygotization, may also
480 contribute. Beyond its evolutionary significance, the *SEM* mechanism has practical
481 implications. Polyploid yeast strains are widely used in fermentation industries,
482 including brewing and baking, and are also frequently isolated from clinical settings
483 (3, 16–18, 47, 48). The identification of the natural mechanism underlying their
484 formation, together with our ability to experimentally recapitulate *SEM*-mediated
485 polyploidization under laboratory conditions without genetic modification, opens
486 new avenues for the rational generation of novel polyploid strains. We envision that
487 controlled and potentially automated implementation of the *SEM* sequence could
488 enable the production of large numbers of polyploids with unprecedented genetic
489 compositions, offering a powerful platform for strain improvement for diverse
490 applications in the food production and fermentation industries.

491 ## Materials and Methods

492 **Strains.** Natural parental diploid (Table S1) and polyploid (Table S5) strains
493 analyzed in this study were obtained from the 1,011 *S. cerevisiae* collection (16) and
494 are referred to using the standardized three-letter strain code. Artificial homozygous
495 polyploids derived from the AKN (YPS128) background, as well as heterozygous
496 polyploids derived from AKN and SACE_YBP (YJM1248) backgrounds (YPB012,
497 YPB022, YPB021), were constructed as described previously (49). Standard reference
498 strains used for ploidy calibration were as previously described (50). Tester strains
499 used for mass mating assays were OS104a and OS104α (YPS128 background) (51).
500

501 **Media composition and growth conditions.** Standard growth medium was YPD,
502 consisting of yeast extract (10 g L^{-1}), peptone (20 g L^{-1}), and dextrose (20 g L^{-1}),
503 prepared with or without agar (20 g L^{-1}). Sporulation medium was potassium acetate
504 (KAc) agar, containing potassium acetate (20 g L^{-1}) and agar (25 g L^{-1}). Selective
505 synthetic complete media were prepared using yeast nitrogen base without
506 ammonium sulfate (YNB; 1.7 g L^{-1}), arginine (2 g L^{-1}), glucose (20 g L^{-1}), and agar (20
507 g L^{-1}), supplemented with appropriate complete supplement mixtures (CSM). CSM
508 + G418 medium contained standard CSM and was supplemented with Geneticin
509 (G418; 200 μg mL^{-1}). CSM - Ura medium contained CSM lacking uracil (CSM - Ura).
510 CSM - Ura + G418 medium was identical to CSM - Ura and additionally
511 supplemented with G418 (200 μg mL^{-1}).
512 Unless otherwise stated, yeast cells were revived from glycerol stocks on YPD agar
513 and grown at 30 °C until the formation of a visible patch prior to experimental
514 assays. Qualitative sporulation and resporulation capacity were assessed by
515 transferring cells to KAc agar and incubating them at 30 °C. After 7 days, cultures
516 were examined by light microscopy for the presence of asci.
517

518 **Flow cytometry.** Cellular ploidy was estimated by propidium iodide staining
519 followed by flow cytometry. Ploidy validations were performed as previously
520 described (50), using cultures grown in YPD. Rapid ploidy assessments were
521 conducted either from overnight 1 mL YPD microcultures or by direct fixation of

522 colonies in 70% ethanol. Flow cytometry data were gated using FSC-A versus SSC-
523 A and FSC-A versus FSC-H to exclude debris and doublets, followed by FSC-A
524 versus PI fluorescence intensity. When required, cell aggregation was reduced by
525 proteinase K treatment. Ploidy values were inferred using MuPETFlow (50) (see
526 Extended Methods).
527
528 **Genotyping mating type loci.** Mating genotype was determined by colony PCR as
529 previously described (34). In a limited number of cases, PCR reactions were
530 performed or repeated using *MAT* locus primers described in (52) to confirm mating
531 genotype assignments.
532
533 **Mass mating assay.** Query and tester cells were mixed on YPD agar and incubated
534 at 30 °C for 24 h to allow mating. Parental query cells were then streaked onto single-
535 selection medium to confirm marker compatibility, while cells from the mating
536 patch were plated onto double-selection medium to assess mating ability (see Media
537 composition and growth conditions).
538
539 **Multi-test screening to detect diploid maters.** All 742 query strains were initially
540 tested using the mass mating assay with minor modifications, and mating outcomes
541 were scored semi-quantitatively, considering as positive only the crosses that
542 formed a confluent cellular layer (see Extended Methods). A subset of 102 strains
543 was further characterized by microscopic examination of zygote formation after 4 h
544 of co-incubation with tester strains, and by assessment of creeping behavior as
545 previously described (53) (see Extended Methods). Results from the three assays
546 were integrated into a single composite mating score, and strains with a score
547 greater than 0 were classified as potential maters. Mating efficiency of candidate
548 strains was then evaluated using a quantitative mating assay adapted from (54).
549 Briefly, equal numbers of query and tester cells (2.5×10^8 cells of each) were mixed
550 and spotted onto a nitrocellulose filter placed on YPD agar. After 4 h of co-
551 incubation at 30 °C, cells were recovered from the filter, serially diluted, and plated
552 onto selective media to quantify colony-forming units (CFUs).

553 Candidate diploid mater strains were subsequently subjected to supplementary
554 analyses to further characterize their mating behavior and genetic features. Mating
555 genotype was determined as described in the section Genotyping mating type loci,
556 and chromosome III aneuploidies and zygosity were retrieved from the original
557 sequencing data (16).
558
559 **Asci dissection and spore isolation.** Sporulated asci were treated with lyticase and
560 dissected using a micromanipulator (Singer Instruments MSM 400) as previously
561 described (34). Spores were plated on YPD agar and cultured at 30 °C, and
562 germination was monitored for up to 7 days. Resulting colonies were picked and
563 stored in glycerol stocks until further analyses.
564
565 **Ascus micromanipulation and polyploid detection.** Complete asci, irrespective of
566 spore number, were randomly isolated and plated onto YPD agar using a
567 micromanipulator (Singer Instruments MSM 400) and incubated at 30 °C. After
568 colony formation (approximately 2 days), a rapid preliminary ploidy assessment
569 was performed as described in the section Flow cytometry. Colonies suspected to be
570 polyploid were subsequently single-colony streaked, and ploidy was validated by
571 flow cytometry.
572
573 **Genomic DNA isolation.** Genomic DNA was extracted either using the E-Z 96
574 Tissue DNA Kit (Omega Bio-Tek), following the manufacturer's instructions, or
575 using the SDS-Kac protocol as previously described (55).
576
577 **Genome sequencing and bioinformatic analysis.** Genomic DNA was sequenced
578 using Illumina paired-end sequencing (2 × 150 bp) with an average insert size of
579 approximately 300 bp. Read quality was assessed using FastQC (v0.12.1) (56) and
580 summarized with MultiQC (v1.13) (57). Read trimming and filtering were
581 performed using Trimmomatic (v0.39) (58), with parallel execution managed using
582 GNU Parallel (v20190322) (59).

583 Read alignment and variant calling were performed using a custom Snakemake-
584 based pipeline (https://github.com/CintiaG/poly_CCN_and_VC.git). Sequencing
585 reads were aligned to the reference genome using BWA (v0.7.18) (60). SAM files
586 were converted to BAM format and sorted using SAMtools (v1.21) (61). Duplicate
587 reads were identified and marked using GATK MarkDuplicatesSpark (v4.5.0.0) (62).
588 Variants were called per strain using GATK HaplotypeCaller in gVCF mode.
589 Individual gVCF files were merged using GATK CombineGVCFs, and joint
590 genotyping was performed with GATK GenotypeGVCFs to generate final VCF files.
591 Chromosome copy number (CCN) was estimated from sequencing depth using
592 BEDTools (v2.29.2) (63). CCN and segmental aneuploidies were inferred using in-
593 house scripts (plot_depth.R and plot_copies.R; https://github.com/CintiaG/wgs-
594 aneuploidy-abr.git).
595 Allele balance ratio (*ABR*) was calculated by extracting read depth (DP) and allele
596 depth (AD) information from VCF files using BCFtools (v1.13) (64). Text outputs
597 were converted to fst format using the fst package (v0.9.8,
598 http://www.fstpackage.org). *ABR* values were computed using the
599 allele_balance_ratio.R script (https://github.com/CintiaG/wgs-aneuploidy-
600 abr.git), retaining variants with *ABR* between 0.125 and 0.875. The number of
601 heterozygous sites was estimated considering only variants with up to three alleles.
602 In selected cases, CCN estimates were manually refined using *ABR* information, and
603 genome-wide visualizations were generated using the plot_allele_balance_ratio.R
604 script (https://github.com/CintiaG/wgs-aneuploidy-abr.git).
605
606 **Data, Materials, and Software Availability.** The data for this study have been
607 deposited in the European Nucleotide Archive (ENA) at EMBL-EBI under accession
608 number PRJEB108394. The genomic data analysis pipeline is deposited at the
609 following repository: https://github.com/CintiaG/wgs-aneuploidy-abr.git
610
611

ACKNOWLEDGMENTS. We are grateful to our colleagues in the *Biology of Genomes* team for their valuable discussions and insights. This work was supported by the Agence Nationale de la Recherche ANR-20-CE12-0020 and ANR-24-CE12-0998.

References

1. J. P. Morris, T. Baslan, D. E. Soltis, P. S. Soltis, D. T. Fox, Integrating the Study of Polyploidy Across Organisms, Tissues, and Disease. *Annu. Rev. Genet.* **58**, 297–318 (2024).
2. A. Selmecki, *et al.*, Polyploidy can drive rapid adaptation in yeast. *Nature* **519**, 349–352 (2015).
3. W. Albertin, P. Marullo, Polyploidy in fungi: evolution after whole-genome duplication. *Proc. R. Soc. B Biol. Sci.* **279**, 2497–2509 (2012).
4. K. A. Segraves, T. J. Anneberg, Species interactions and plant polyploidy. *Am. J. Bot.* **103**, 1326–1335 (2016).
5. T. E. Wood, *et al.*, The frequency of polyploid speciation in vascular plants. *Proc. Natl. Acad. Sci.* **106**, 13875–13879 (2009).
6. B. K. MABLE, 'Why polyploidy is rarer in animals than in plants': myths and mechanisms. *Biol. J. Linn. Soc.* **82**, 453–466 (2004).
7. B. K. Mable, M. A. Alexandrou, M. I. Taylor, Genome duplication in amphibians and fish: an extended synthesis. *J. Zool.* **284**, 151–182 (2011).
8. K. T. David, Global gradients in the distribution of animal polyploids. *Proc. Natl. Acad. Sci. U. S. A.* **119**, e2214070119 (2022).
9. M. Mezzasalma, E. Brunelli, G. Odierna, F. M. Guarino, Evolutionary and Genomic Diversity of True Polyploidy in Tetrapods. *Anim. Open Access J. MDPI* **13**, 1033 (2023).
10. C. M. Bielski, *et al.*, Genome doubling shapes the evolution and prognosis of advanced cancers. *Nat. Genet.* **50**, 1189–1195 (2018).
11. R. A. Lambuta, *et al.*, Whole-genome doubling drives oncogenic loss of chromatin segregation. *Nature* **615**, 925–933 (2023).
12. F. Martínez-Jiménez, *et al.*, Pan-cancer whole-genome comparison of primary and metastatic solid tumours. *Nature* **618**, 333–341 (2023).
13. S. P. Otto, J. Whitton, Polyploid incidence and evolution. *Annu. Rev. Genet.* **34**, 401–437 (2000).
14. J. Ramsey, D. W. Schemske, PATHWAYS, MECHANISMS, AND RATES OF POLYPLOID FORMATION IN FLOWERING PLANTS. *Annu. Rev. Ecol. Evol. Syst.* **29**, 467–501 (1998).
15. C. M. Ward, *et al.*, Recombination, admixture and genome instability shape the genomic landscape of Saccharomyces cerevisiae derived from spontaneous grape ferments. *PLOS Genet.* **20**, e1011223 (2024).
16. J. Peter, *et al.*, Genome evolution across 1,011 Saccharomyces cerevisiae isolates. *Nature* **556**, 339 (2018).
17. S.-F. Duan, *et al.*, The origin and adaptive evolution of domesticated populations of yeast from Far East Asia. *Nat. Commun.* **9**, 2690 (2018).
18. V. Loegler, A. Friedrich, J. Schacherer, Overview of the Saccharomyces cerevisiae population structure through the lens of 3,034 genomes. *G3 Bethesda Md* **14**, jkae245 (2024).
19. G. Fischer, G. Liti, B. Llorente, The budding yeast life cycle: More complex than anticipated? *Yeast Chichester Engl.* **38**, 5–11 (2021).
20. S. Pomper, K. M. Daniels, D. W. McKee, Genetic Analysis of Polyploid Yeast. *Genetics* **39**, 343–355 (1954).

21. N. Gunge, Y. Nakatomi, Genetic Mechanisms of Rare Matings of the Yeast SACCHAROMYCES CEREVISIAE Heterozygous for Mating Type. *Genetics* **70**, 41–58 (1972).
22. K. H. Wolfe, D. C. Shields, Molecular evidence for an ancient duplication of the entire yeast genome. *Nature* **387**, 708–713 (1997).
23. M. Marcet-Houben, T. Gabaldón, Beyond the Whole-Genome Duplication: Phylogenetic Evidence for an Ancient Interspecies Hybridization in the Baker's Yeast Lineage. *PLOS Biol.* **13**, e1002220 (2015).
24. S. Marsit, M. Hénault, G. Charron, A. Fijarczyk, C. R. Landry, The neutral rate of whole-genome duplication varies among yeast species and their hybrids. *Nat. Commun.* **12**, 3126 (2021).
25. G. Charron, S. Marsit, M. Hénault, H. Martin, C. R. Landry, Spontaneous whole-genome duplication restores fertility in interspecific hybrids. *Nat. Commun.* **10**, 1–10 (2019).
26. K. Tong, *et al.*, Genome duplication in a long-term multicellularity evolution experiment. *Nature* **639**, 691–699 (2025).
27. V. W. Mayer, A. Aguilera, High levels of chromosome instability in polyploids of Saccharomyces cerevisiae. *Mutat. Res.* **231**, 177–186 (1990).
28. A. C. Gerstein, H.-J. E. Chun, A. Grant, S. P. Otto, Genomic convergence toward diploidy in Saccharomyces cerevisiae. *PLoS Genet.* **2**, e145 (2006).
29. A. C. Gerstein, R. M. McBride, S. P. Otto, Ploidy reduction in Saccharomyces cerevisiae. *Biol. Lett.* **4**, 91–94 (2008).
30. A. Dutta, F. Dutreux, J. Schacherer, Loss of Heterozygosity Spectrum Depends on Ploidy Level in Natural Yeast Populations. *Mol. Biol. Evol.* **39**, msac214 (2022).
31. D. T. Fox, R. J. Duronio, Endoreplication and polyploidy: insights into development and disease. *Development* **140**, 3–12 (2013).
32. B. A. Edgar, T. L. Orr-Weaver, Endoreplication Cell Cycles: More for Less. *Cell* **105**, 297–306 (2001).
33. Y. Harari, Y. Ram, N. Rappoport, L. Hadany, M. Kupiec, Spontaneous Changes in Ploidy Are Common in Yeast. *Curr. Biol. CB* **28**, 825-835.e4 (2018).
34. N. Vittorelli, *et al.*, Repeated losses of self-fertility shaped heterozygosity and polyploidy in yeast evolution. *Proc. Natl. Acad. Sci.* **123**, e2525679123 (2026).
35. M. De Chiara, *et al.*, Domestication reprogrammed the budding yeast life cycle. *Nat. Ecol. Evol.* **6**, 448–460 (2022).
36. J. St. Charles, M. L. Hamilton, T. D. Petes, Meiotic Chromosome Segregation in Triploid Strains of Saccharomyces cerevisiae. *Genetics* **186**, 537–550 (2010).
37. S. Mozzachiodi, K. Krogerus, B. Gibson, A. Nicolas, G. Liti, Unlocking the functional potential of polyploid yeasts. *Nat. Commun.* **13**, 2580 (2022).
38. J. Barrere, P. Nanda, A. W. Murray, Alternating selection for dispersal and multicellularity favors regulated life cycles. *Curr. Biol. CB* **33**, 1809-1817.e3 (2023).
39. J. Loidl, Meiotic chromosome pairing in triploid and tetraploid Saccharomyces cerevisiae. *Genetics* **139**, 1511–1520 (1995).
40. J. E. Haber, BISEXUAL MATING BEHAVIOR IN A DIPLOID OF SACCHAROMYCES CEREVISIAE: EVIDENCE FOR GENETICALLY

CONTROLLED NON-RANDOM CHROMOSOME LOSS DURING VEGETATIVE GROWTH. *Genetics* **78**, 843–858 (1974).

41. R. Al Safadi, M. Weiss-Gayet, J. Briolay, M. Aigle, A polyploid population of Saccharomyces cerevisiae with separate sexes (dioecy). *FEMS Yeast Res.* **10**, 757–768 (2010).
42. G. Pan, Y. Zhou, L. C. Fowke, H. Wang, An efficient method for flow cytometric analysis of pollen and detection of 2n nuclei in Brassica napus pollen. *Plant Cell Rep.* **23**, 196–202 (2004).
43. D. Schild, H. N. Ananthaswamy, R. K. Mortimer, An endomitotic effect of a cell cycle mutation of Saccharomyces cerevisiae. *Genetics* **97**, 551–562 (1981).
44. Y. Andreychuk, A. Zhuk, E. Tarakhovskaya, S. Inge-Vechtomov, E. Stepchenkova, Rate of spontaneous polyploidization in haploid yeast Saccharomyces cerevisiae. *Biol. Commun.* **67**, 88–96 (2022).
45. S. Tung, C. W. Bakerlee, A. M. Phillips, A. N. Nguyen Ba, M. M. Desai, The genetic basis of differential autodiploidization in evolving yeast populations. *G3 GenesGenomesGenetics* **11**, jkab192 (2021).
46. J. Hose, *et al.*, The genetic basis of aneuploidy tolerance in wild yeast. *eLife* **9**, e52063 (2020).
47. T. K. Ezov, *et al.*, Molecular-Genetic Biodiversity in a Natural Population of the Yeast Saccharomyces cerevisiae From "Evolution Canyon": Microsatellite Polymorphism, Ploidy and Controversial Sexual Status. *Genetics* **174**, 1455–1468 (2006).
48. L. A. H. Muller, J. H. McCusker, Microsatellite analysis of genetic diversity among clinical and nonclinical Saccharomyces cerevisiae isolates suggests heterozygote advantage in clinical environments. *Mol. Ecol.* **18**, 2779–2786 (2009).
49. C. Garrido, *et al.*, Natural diversity of telomere length distributions across 100 Saccharomyces cerevisiae strains. *Genome Res.* gr.281132.125 (2026). https://doi.org/10.1101/gr.281132.125.
50. C. Gómez-Muñoz, G. Fischer, MuPETFlow: multiple ploidy estimation tool from flow cytometry data. *BMC Genomics* **26**, 301 (2025).
51. F. A. Cubillos, E. J. Louis, G. Liti, Generation of a large set of genetically tractable haploid and diploid Saccharomyces strains. *FEMS Yeast Res.* **9**, 1217–1225 (2009).
52. C. Huxley, E. D. Green, I. Dunham, Rapid assessment of S. cerevisiae mating type by PCR. *Trends Genet. TIG* **6**, 236 (1990).
53. S. D. M. Arras, *et al.*, Creeping yeast: a simple, cheap and robust protocol for the identification of mating type in Saccharomyces cerevisiae. *FEMS Yeast Res.* **22**, foac017 (2022).
54. M. de Barros Lopes, J. R. Bellon, N. J. Shirley, P. F. Ganter, Evidence for multiple interspecific hybridization in *Saccharomyces* sensu stricto species. *FEMS Yeast Res.* **1**, 323–331 (2002).
55. N. Agier, *et al.*, A transient mutational burst occurs during yeast colony development. *Mol. Syst. Biol.* **21**, 1214–1236 (2025).
56. Andrews, S. (2010) FastQC A Quality Control Tool for High Throughput Sequence Data. - References - Scientific Research Publishing. Available at:

https://www.scirp.org/reference/referencespapers?referenceid=2781642 [Accessed 11 January 2026].

57. P. Ewels, M. Magnusson, S. Lundin, M. Käller, MultiQC: summarize analysis results for multiple tools and samples in a single report. *Bioinforma. Oxf. Engl.* **32**, 3047–3048 (2016).
58. A. M. Bolger, M. Lohse, B. Usadel, Trimmomatic: a flexible trimmer for Illumina sequence data. *Bioinforma. Oxf. Engl.* **30**, 2114–2120 (2014).
59. GNU Parallel 2018. *Guide Books*. Available at: https://dl.acm.org/doi/abs/10.5555/3235180 [Accessed 11 January 2026].
60. H. Li, R. Durbin, Fast and accurate short read alignment with Burrows–Wheeler transform. *Bioinformatics* **25**, 1754–1760 (2009).
61. H. Li, *et al.*, The Sequence Alignment/Map format and SAMtools. *Bioinforma. Oxf. Engl.* **25**, 2078–2079 (2009).
62. G. A. Van der Auwera, *et al.*, From FastQ data to high confidence variant calls: the Genome Analysis Toolkit best practices pipeline. *Curr. Protoc. Bioinforma.* **43**, 11.10.1-11.10.33 (2013).
63. A. R. Quinlan, I. M. Hall, BEDTools: a flexible suite of utilities for comparing genomic features. *Bioinforma. Oxf. Engl.* **26**, 841–842 (2010).
64. P. Danecek, S. A. McCarthy, BCFtools/csq: haplotype-aware variant consequences. *Bioinformatics* **33**, 2037–2039 (2017).

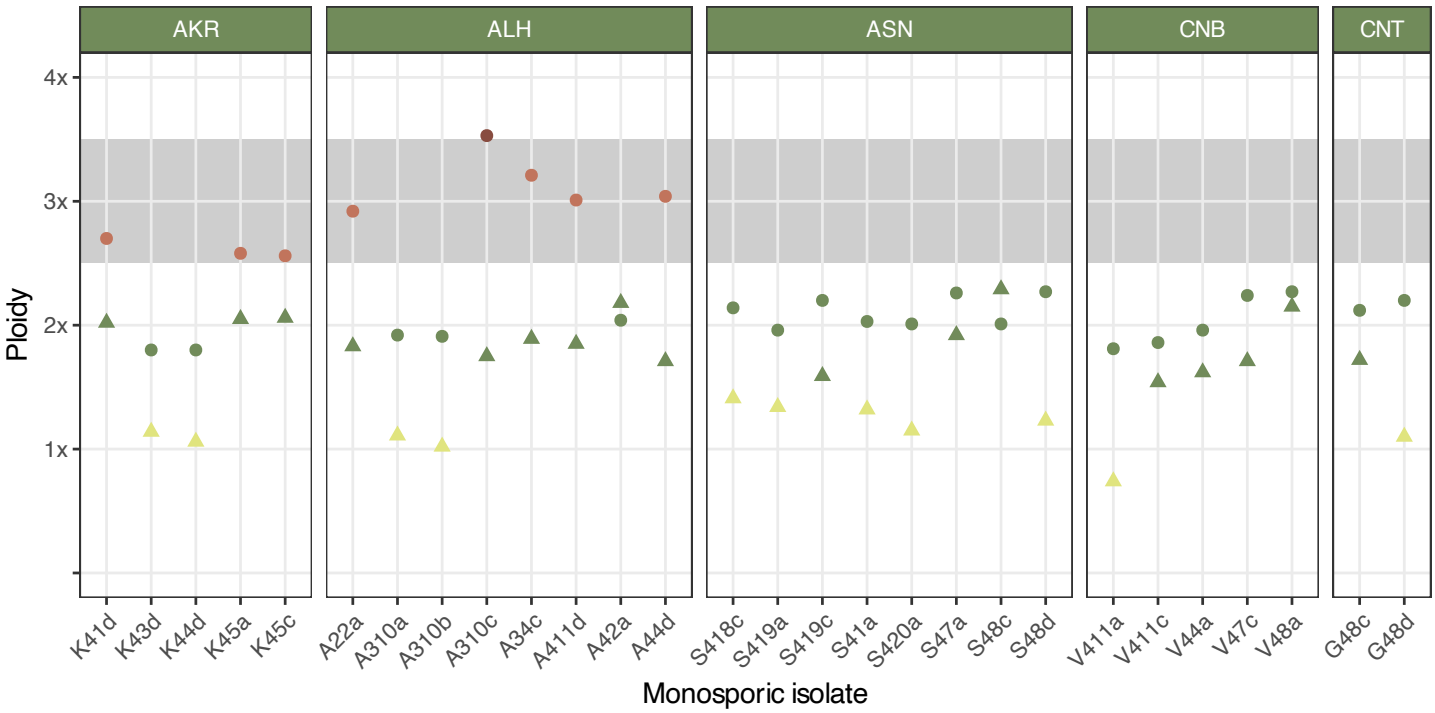

Supplementary figure 1

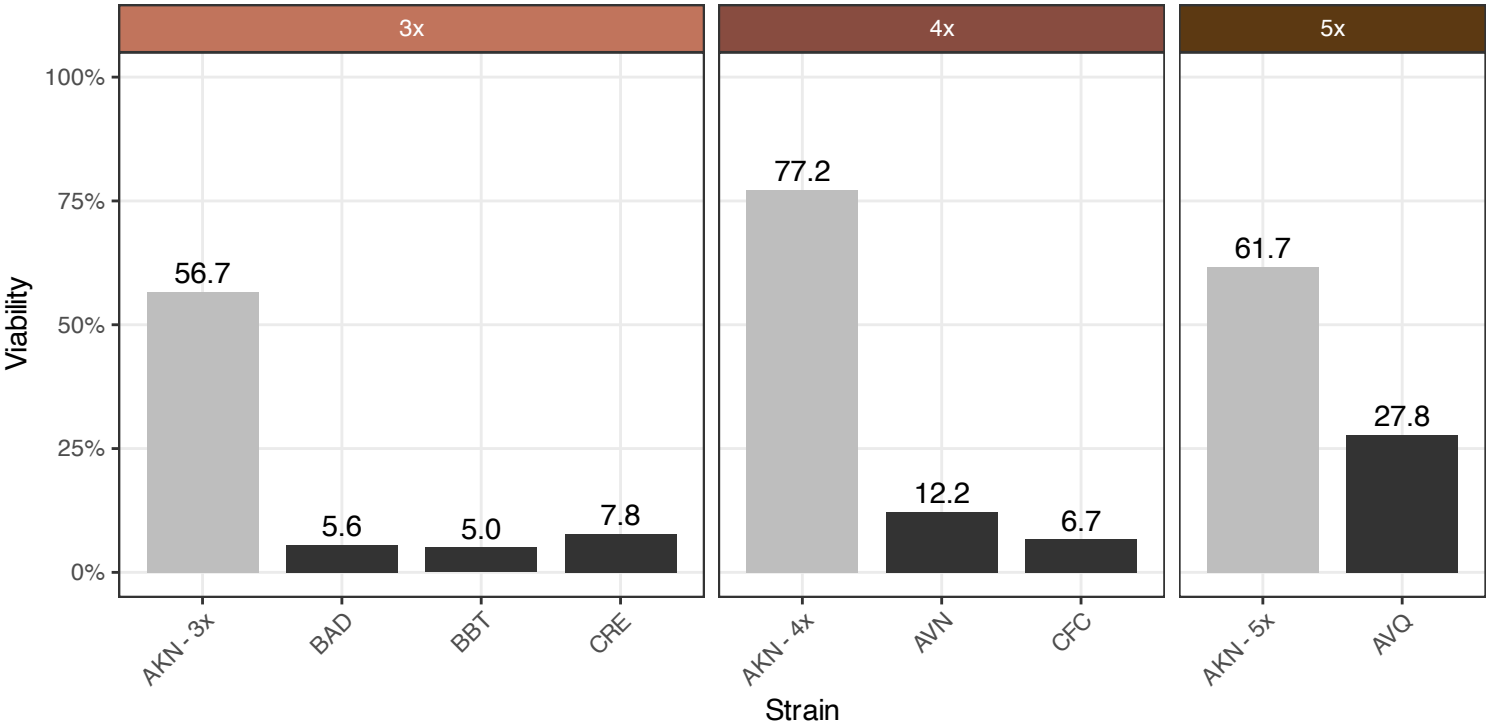

Supplementary figure 2

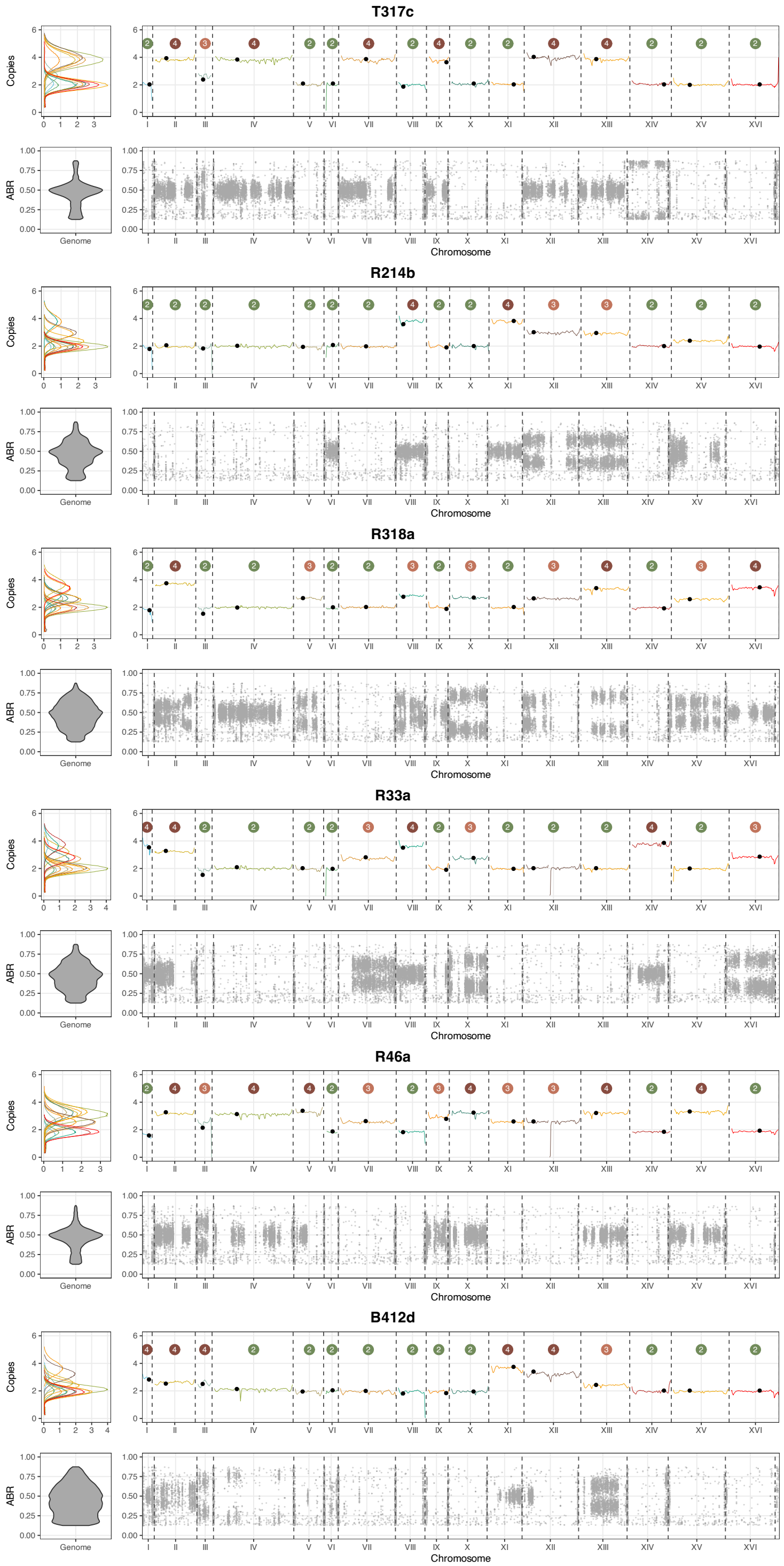

Supplementary figure 3

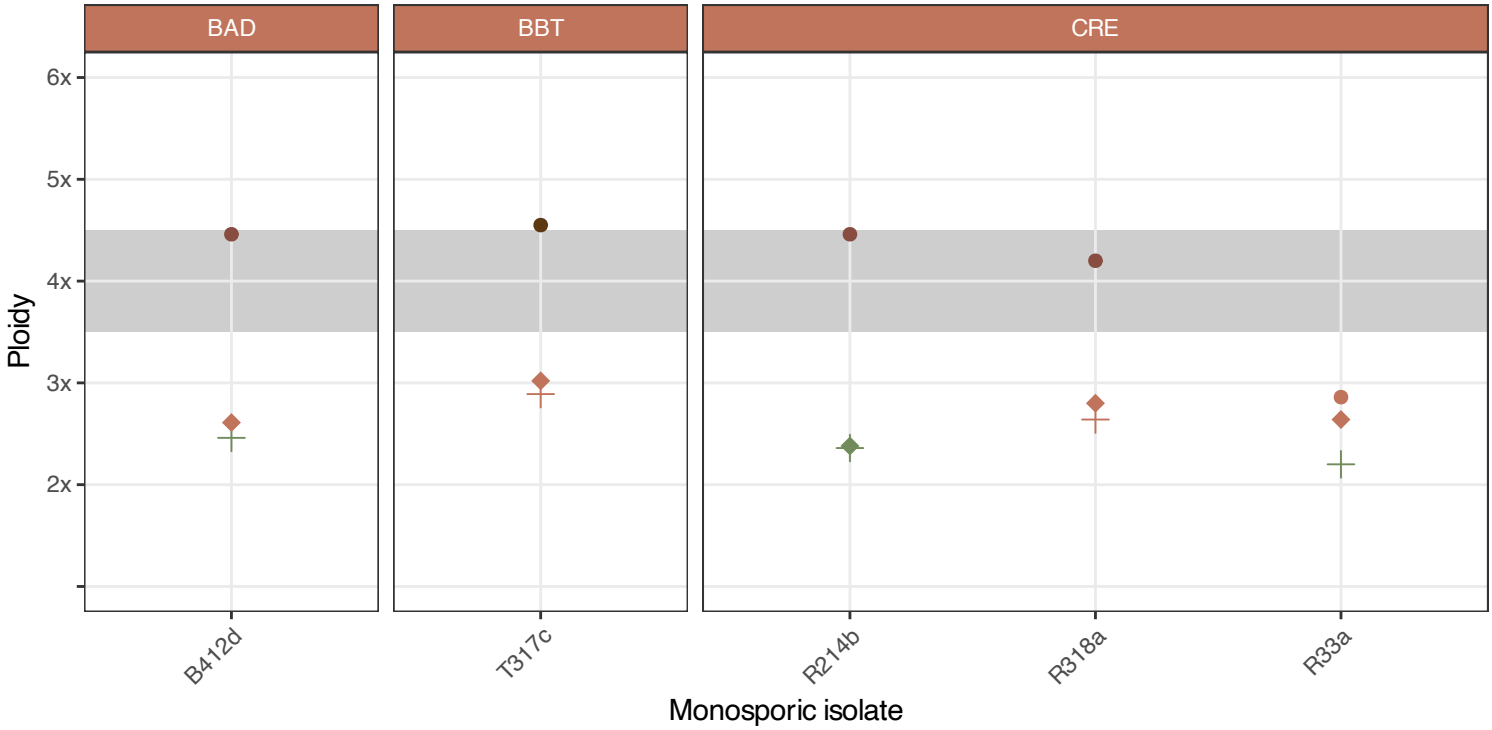

Supplementary figure 4

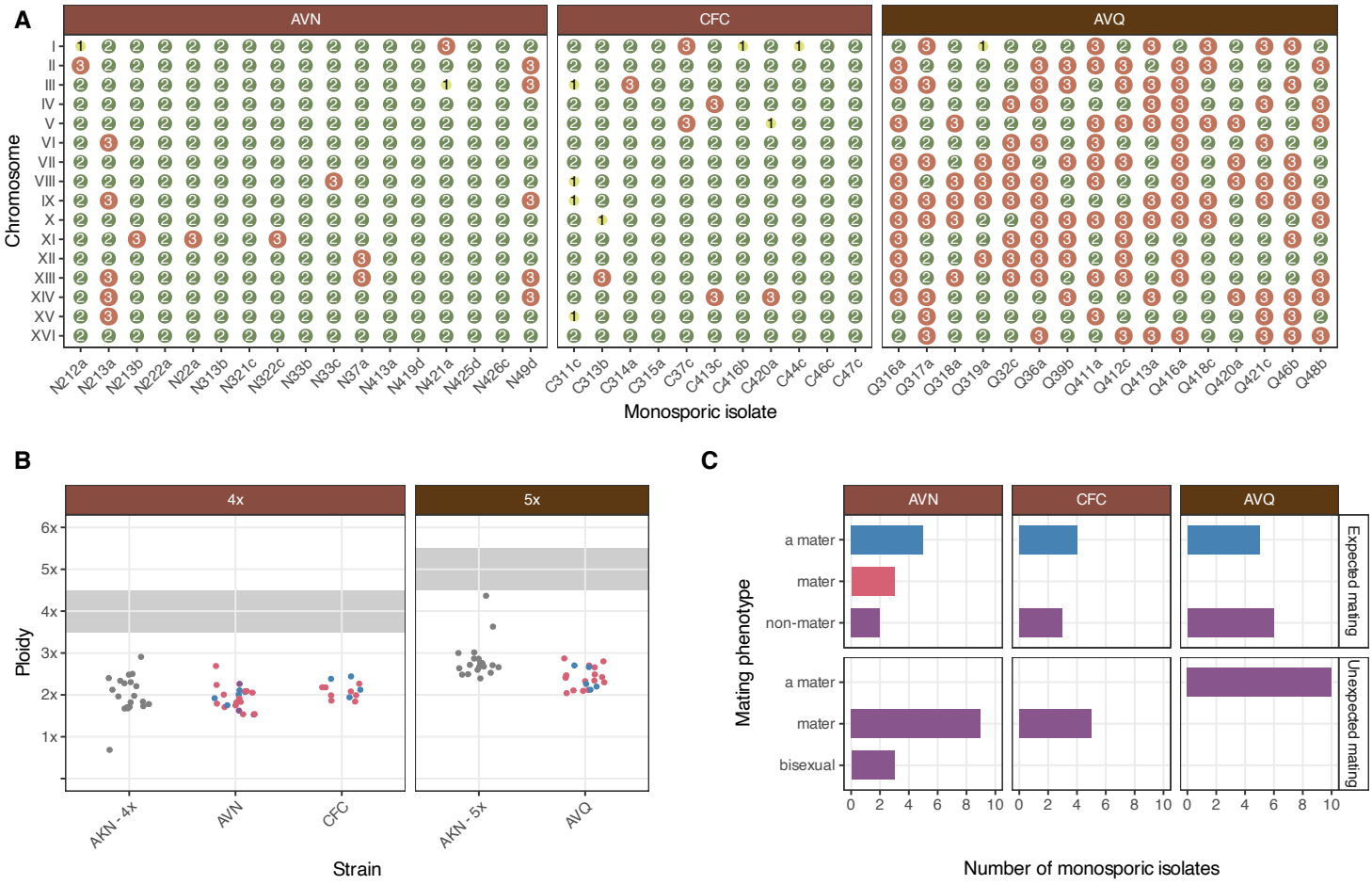

Supplementary figure 5

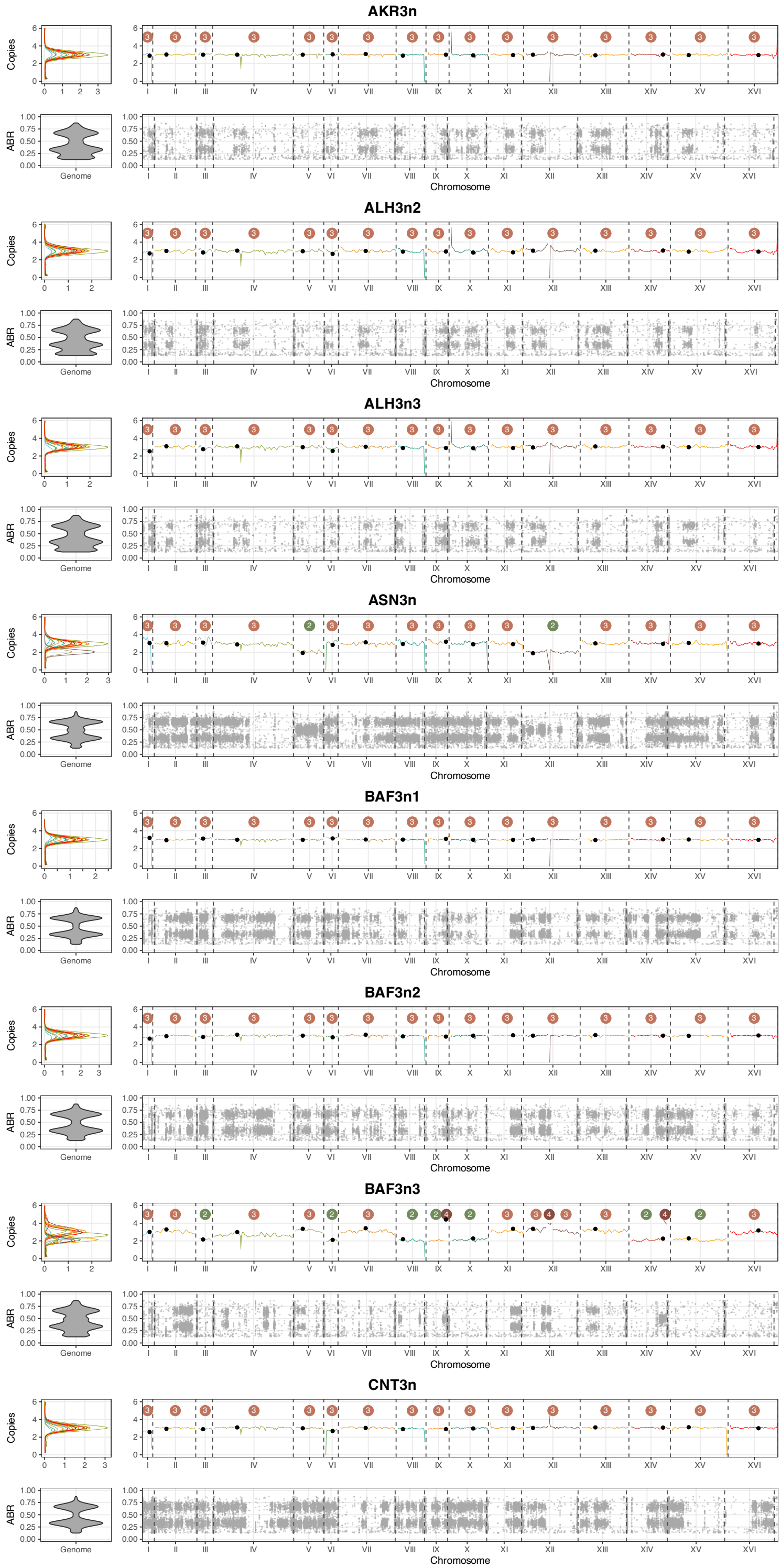

Supplementary figure 6

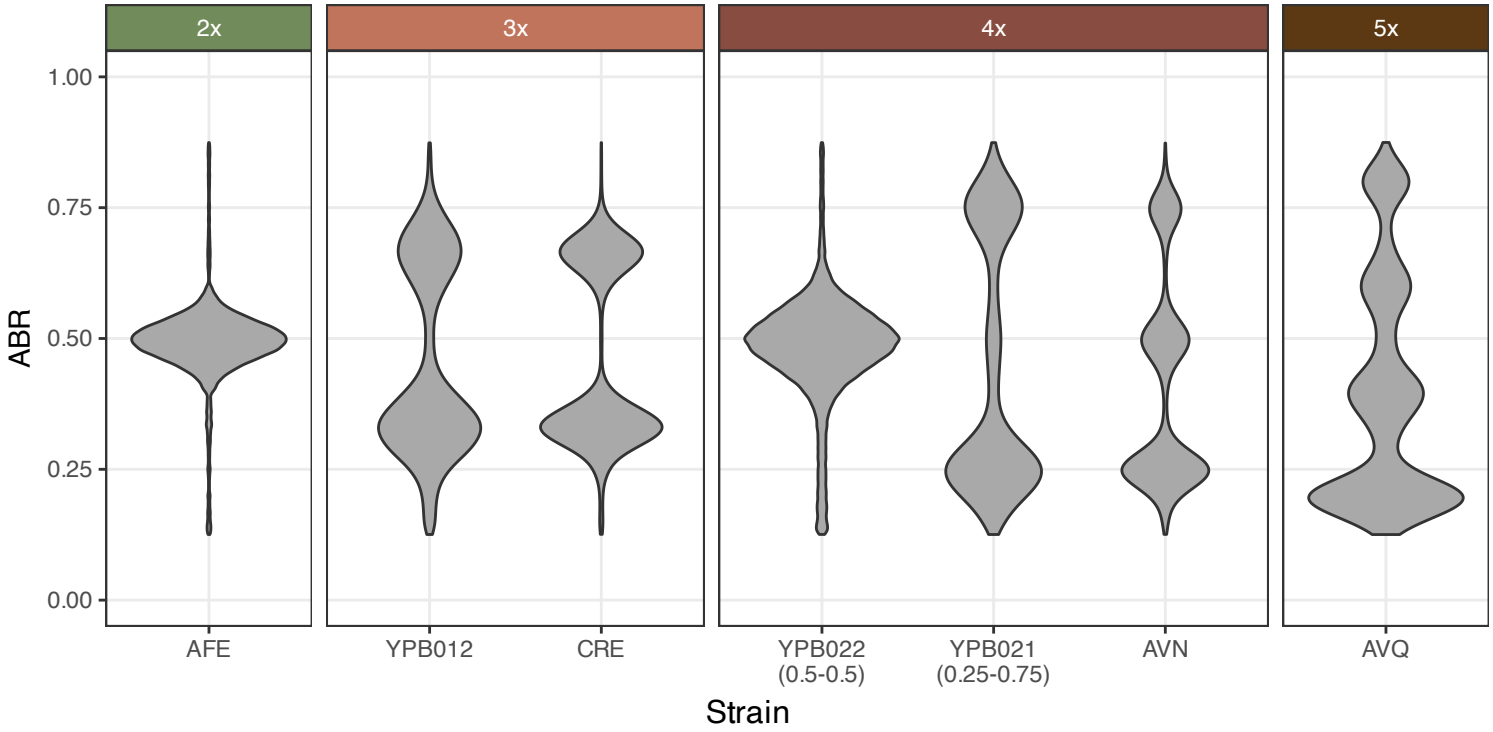

Supplementary figure 7

Legends to Supplementary Figures:

Supplementary Figure 1. Ploidy of monosporic isolates derived from diploid strains (triangles) and their progeny following crosses with compatible haploid testers (circles). Measurements are colored according to the rounded ploidy value: yellow, haploid; green, diploid; orange, triploid; and red, tetraploid. The shaded gray area indicates the expected ploidy range of triploids originating from endoreplicated spores. Monosporic isolates from strains AKR and ALH produced triploid progeny.

Supplementary Figure 2. Spore viability of artificial homozygous (light gray) and natural heterozygous polyploid strains (dark gray) of varying ploidy. Viability values were inferred from 180 dissected spores per strain. The reduced viability observed in natural strains likely reflects the combined effects of chromosome missegregation and mutational load.

Supplementary Figure 3. Whole-genome profiles of monosporic isolates derived from endoreplicated triploids. Sequencing depth histograms (top left panel) were used to estimate chromosome copy number (top right panel; values indicated above each chromosome). Centromeres are marked with black circles. Allele balance ratio (ABR) profiles are shown at the genome-wide level (bottom left panel) and per chromosome (bottom right panel), with only alternative alleles plotted. Endoreplicated monosporic isolates exhibited substantial levels of homozygous disomes and heterozygous tetrasomes, the latter characterized by an ABR of 0.5.

Supplementary Figure 4. Ploidy of monosporic isolates derived from triploid strains (crosses), bioinformatically estimated ploidy (diamonds), and their progeny following crosses with compatible haploid testers (circles). Bioinformatic ploidy was calculated by estimating chromosome copy number from sequencing depth and summing the product of copy number and chromosome length across all chromosomes. Measurements are colored according to the rounded ploidy value: green, diploid; orange, triploid; red, tetraploid; and dark red, pentaploid. The shaded gray area highlights the approximate ploidy threshold observed for the crosses.

Supplementary Figure 5. A, Chromosome copy number profiles of monosporic isolates derived from tetraploid (AVN and CFC) and pentaploid (AVQ) strains. No evidence of post-meiotic endoreplication was detected. B, Inferred ploidy distributions of monosporic isolates; shaded areas indicate the expected ploidy range of endoreplicated isolates, which was not observed. C, Mating genotypes and mating phenotypes of monosporic isolates derived from tetraploid and pentaploid strains. These isolates exhibited mating activity and, given their initial ploidy, could reconstitute the parental ploidy.

Supplementary Figure 6. Whole-genome profiles of spontaneous triploids recovered from intra-ascus mating of spores derived from diploid strains. Sequencing depth histograms (top left panel) were used to estimate chromosome copy number (top right panel; values indicated above each chromosome). Centromeres are marked with black circles. Allele balance ratio (ABR) profiles are shown at the genome-wide level (bottom left panel) and per chromosome (bottom right panel), with only alternative alleles plotted. The recovered isolates exhibited major genome-wide ABR values of 0.33 and 0.66, consistent with their triploid nature.

Supplementary Figure 7. Allele balance ratio (ABR) profiles of *Saccharomyces cerevisiae* strains with varying ploidy. Only alternative alleles are plotted. Diploid heterozygous strains exhibit a single ABR value of 0.5. Polyploids display characteristic discrete ABR values: multiples of 0.33 for triploids, 0.25 for tetraploids, and 0.2 for pentaploids. Notably, the ABR profiles of natural tetraploids differed from those of artificial tetraploids, presenting all combinations of 0.25 multiples.

Extended Methods

Ploidy analysis by flow cytometry details

Cellular ploidy was estimated by propidium iodide (PI) staining coupled with flow cytometry. For ploidy validation experiments, strains were grown in 5 mL YPD at 30 °C and processed as previously described[1]. For rapid ploidy assessment, either overnight 1 mL YPD microcultures were prepared prior to fixation, or individual colonies were directly fixed in 70% ethanol.

Fixed cells were stained with PI (50 μg mL^{-1}) and analyzed using a MACSQuant VYB flow cytometer. Data were processed using CytoExploreR (https://github.com/DillonHammill/CytoExploreR). Initial gating was performed using forward scatter area (FSC-A) versus side scatter area (SSC-A) to exclude debris, followed by FSC-A versus FSC-H to eliminate doublets. To mitigate cell aggregation, two complementary strategies were employed. First, selected samples were subjected to a proteinase K treatment (5 mg mL^{-1}) for 2 h at 50 °C prior to staining. Second, an additional gating step using FSC-A versus PI fluorescence intensity (FL4-A; 605-625 nm) was applied. Samples in which more than 50% of events fell within this third gate were considered to yield reliable ploidy estimates. Information regarding proteinase K treatment and gating quality metrics is reported in Table S2 (columns "Proteinase" and "Cells_gate").

G0/G1 and G2 PI fluorescence intensity peaks were quantified and summarized using MuPETFlow (v0.1.1)[1]. Both decimal and rounded ploidy values were extracted and used for downstream analyses.

Mass mating assays details

Query and tester strains were grown on YPD agar prior to mating. Using a sterile 1-μL inoculation loop, a small amount of cells from each query and tester strain was streaked separately onto defined 1 cm^2 areas of YPD agar plates. Approximately half of the cells from each strain were then mixed together in the 1 cm^2 area between the two streaks, while portions of each culture were left unmixed and served as internal controls.

Plates were incubated for 24h at 30 °C to allow mating. A panel of selective media was used as described in the Media composition and growth conditions section. After incubation, cells from the mixed mating zone were collected using a sterile toothpick and streaked onto double-selection medium (CSM - Ura + G418) using the three-streak dilution method to obtain isolated colonies. In parallel, tester strains were streaked

onto single-selection media (CSM - Ura and CSM + G418) to verify marker compatibility (uracil prototrophy and G418 sensitivity) and growth.

Plates were incubated at 30 °C and examined after 3 days. Crosses were scored as positive when multiple colonies were observed on the double-selection medium beyond the initial inoculation streak.

To enable higher-throughput detection of diploid maters, the standard mass mating protocol was modified. Tester and query strains were first resuspended in liquid YPD, mixed, spotted onto YPD agar, and incubated at 30 °C for the same duration as in the standard assay.

After mating incubation, cells were not streaked. Instead, a small amount of cells was collected using a sterile 1-μL inoculation loop, resuspended in 1 mL sterile H_2O, and diluted 1:10. Diluted suspensions were then spotted onto double-selection medium.

Zygote formation and creeping assays

For the zygote formation assay, a small amount of cells from the query strain was mixed with tester strains and incubated for 4 h. Samples were then examined by light microscopy for the presence of zygotes, identified as buds emerging from two fused cells.

Creeping assays were performed as described previously[2]. Briefly, 100 μL of query and tester cell suspensions adjusted to an optical density of 0.2 were mixed in flat-bottom 96-well plates and incubated for 16 h. Creeping behavior was scored based on the formation of a growth ring along the wall of the well.

Mating score calculation

Mating efficiency was first assessed semi-quantitatively using the following scoring scheme: no growth (score 0), poor growth (1–10 colonies; score 1), moderate growth (11–50 colonies; score 2), sparse cell layer (score 3), and confluent cell layer (score 4). For each strain, results were recorded as a pair of scores corresponding to crosses with the *a* and *α* tester strains, respectively. Accordingly, a result of (0/4) indicates no mating with the *MATa* tester but robust mating with the *MATα* tester, consistent with an *a* mater phenotype. Semi-quantitative mass mating scores were then converted into partial scores of -1, 0, or 1. Scores below 3 were assigned -1, scores equal to 3 were assigned 0, and only a score of 4 was assigned 1, to restrict the analysis to strains displaying clear mating signals. Zygote formation assays were scored as 1 for positive and -1 for negative outcomes. For creeping assays, positive results were assigned a score of 1, whereas negative results were assigned 0, as weak positive signals may not be reliably detected by this assay. When assays were performed in replicate, partial

scores from each replicate were summed and averaged. Discrepant replicates therefore yielded intermediate decimal values. Final mating scores were obtained by summing all partial scores as follows:

Mass mating		Zygote formation		Creeping	
Result	Partial score	Result	Partial score	Result	Partial score
4	1	Positive	1	Positive	1
3	0	Negative	-1	Negative	0
2	-1				
1	-1				
0	-1				

Quantitative mating assay

Mating efficiency was quantified using an assay adapted from[3]. Query and tester strains were grown on YPD agar, resuspended in liquid medium, and optical density at 600 nm was measured. For each cross, a volume corresponding to 2.5×10^8 cells of each strain was collected by centrifugation and resuspended in 125 μL of sterile 1× PBS.

Equal volumes of query and tester cell suspensions were mixed to obtain a final volume of 250 μL per mating mix. Each mating mix was briefly sonicated (20% amplitude, 15 s) to disrupt cell aggregates. Nitrocellulose filters (7 mm diameter) were placed onto YPD agar, and 5 μL of each mating mix was spotted onto the corresponding filter. Filters were incubated for 4 h at 30 °C to allow mating.

After incubation, each filter was transferred into 1 mL of sterile 1× PBS and vortexed to resuspend cells. Serial dilutions were prepared and plated onto double-selection medium (CSM - Ura + G418) to quantify mating products. Plates were incubated at 30 °C for 3-4 days, after which colonies were counted to calculate colony-forming units (CFUs).

References

1. Gómez-Muñoz, C. & Fischer, G. MuPETFlow: multiple ploidy estimation tool from flow cytometry data. *BMC Genomics* **26**, 301 (2025).
2. Arras, S. D. M. *et al.* Creeping yeast: a simple, cheap and robust protocol for the identification of mating type in Saccharomyces cerevisiae. *FEMS Yeast Res.* **22**, foac017 (2022).
3. de Barros Lopes, M., Bellon, J. R., Shirley, N. J. & Ganter, P. F. Evidence for multiple interspecific hybridization in *Saccharomyces* sensu stricto species. *FEMS Yeast Res.* **1**, 323–331 (2002).